Journal of Marine Research, 55, 1199–1251, 1997

Circulation around islands and ridges

by Joseph Pedlosky[1], Lawrence J. Pratt[1], Michael A. Spall[1] and Karl R. Helfrich[1]

ABSTRACT

The circulation in an ocean basin containing an island is studied under nearly geostrophic, beta plane dynamics. The model is a fluid of uniform density driven by wind forcing or sources and sinks of mass at the upper boundary of the flow. The circulation is studied analytically, numerically, as well as in the laboratory through the device of the "sliced cylinder" model for the ocean circulation. Of particular interest is the estimate of the transport between the island and the oceanic basin's boundary. The model is conceived as relevant to both the wind-driven circulation as well as the circulation of abyssal waters around deep topographic features such as mid-ocean ridge segments.

Godfrey's Island Rule for the transport is re-derived in general form and the validity of the original approximation of Godfrey (1989) is examined in a variety of circumstances. In particular, the role of dissipative boundary layers and inertial effects such as vortex shedding are scrutinized to determine their role in determining the net transport around the island.

Linear theory in many cases predicts a recirculation on the eastern side of the island, provided the meridional extent of the island is large enough. The existence of the recirculation, containing trapped fluid, is confirmed in both laboratory and numerical experiments and the evolution of the structure of the recirculation is examined as a function of the boundary layer Reynolds number. In both the laboratory and numerical studies, the recirculation predicted by linear theory is joined and then superseded by an inertial recirculation springing from boundary layer separation as the Reynolds number increases past a critical value.

Even in the linear limit it is shown that the recirculation region, which is closed in quasi-geostrophic theory, is subject to a small leak due to planetary geostrophic effects, which prediction is confirmed in the laboratory.

The original island rule of Godfrey yields an estimate of the transport which is surprisingly robust and generally within 75% of the values measured in our numerical experiments. Agreement is moderately good when island western boundary layer transport is used as a basis for comparison. Several cases are discussed, however, in which the assumptions made by Godfrey are violated. One occurs when the frictional boundary layers of the island and the basin boundary overlap. We derive a threshold width for the gap for the case where the island is close to a northern or southern boundary of the basin and show how the transport is increasingly blocked as the gap is reduced. A second case occurs when the island is thin and zonally elongated so that the dissipative effects on the northern and southern boundaries of the island become important. Here the vorticity balance assumed in the simple Island Rule is fundamentally altered, and we extend the Island Rule to account for the new dissipation.

1. Woods Hole Oceanographic Institution, Woods Hole, Massachusetts, 02543, U.S.A.

1. Introduction

An island within an ocean basin introduces a new quantity to the solution of the problem of the general circulation in the basin. This is the total transport between the island and the external boundary of the basin. If the circulation is in a steady state, the transport around the island must be the same all around the island; i.e., between any point on the island's boundary and the basin's outer boundary. Thus, this new part of the solution is represented by a single constant. Mathematically, the ocean with an island is a multiply connected region and this gives rise to novel physical features in the dynamical problem for the circulation manifested by the need to determine the constant transport around the island.

For example, if we model the circulation as a two-dimensional barotropic flow governed by a streamfunction ψ, this streamfunction must be constant on both the boundary of the island and the outer boundary of the basin in order to satisfy the no-normal flow condition on each boundary. We may arbitrarily choose the value of that constant on one boundary. Thus we may choose $\psi = 0$ on the basin's outer boundary, but the value of $\psi = \psi_I$ on the island's boundary must be determined as part of the solution of the problem since its value gives the total clockwise, barotropic transport between the island and the basin's perimeter. A prominent example is the calculation of the net northward transport between Australia and South America (Godfrey, 1989), the value of which also serves as an estimate of the Indo-Pacific throughflow transport.

In order to determine the additional part of the solution associated with the value of ψ on the island boundary it is necessary to consider the equation for the fluid circulation, Γ, around the island's perimeter, C_I, where

$$\Gamma = \oint_{C_I} \boldsymbol{u} \cdot \hat{t}\, ds, \tag{1.1}$$

where $\hat{t}$ is a unit tangent vector to the island as shown in Figure 1 and ds is the differential distance along C_I. The balance of tangential forces which enter to determine the circulation around the island includes the dissipation on the eastern side of the island and this leads to both theoretical and observational challenges in the attempt to determine ψ_I. To determine the dissipative force requires a detailed analysis of the boundary layer on the island's eastern boundary. This is a western boundary layer region for the sub-basin between the island and the ocean's eastern boundary, and strong currents and substantial dissipation can be expected in this region. This is difficult to calculate theoretically or observe directly in the ocean. Godfrey (1989) introduced an altered contour, shown as C in Figure 1, which runs from the eastern boundary of the basin along latitudes which brush the northern and southern extremities of the island and enfolds the western side of the island and then closes along the basin's eastern boundary. Godfrey showed the dynamical equivalence of the two contours which allows ψ_I to be determined using C. This ingenious device avoids dealing with the details of the western boundary layer on the eastern side of the island and gives rise to an explicit prediction for the transport around the island; i.e., it yields the constant ψ_I on the island. Godfrey showed that in the approximation when the dynamics were linear,

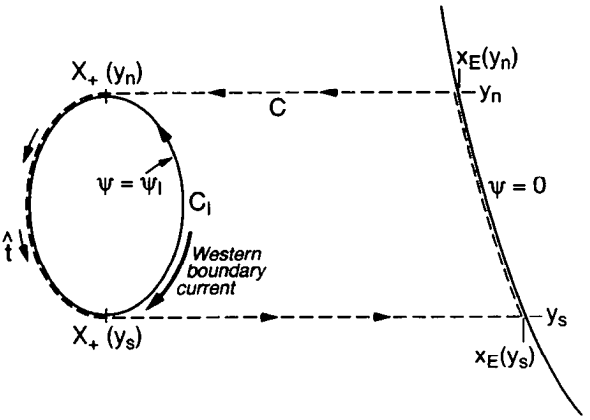

Figure 1. The general configuration of the island in a basin. The northern and southern extremities of the island are given by y_n and y_s, respectively. The integration contour around the island is C_I. The eastern boundary of the basin is at $x_e(y)$. The extended contour which runs along the latitudes y_n and y_s and enfolds the western perimeter of the island and then closes along the eastern boundary is C. The tangent unit vector to either contour, defined locally, is $\hat{t}$.

the motion was steady, and dissipation could be ignored everywhere but in the boundary layer on the eastern side of the island, the transport ψ_I is given by

$$[f(y_n) - f(y_s)]\,\psi_I = -\oint_C \left(\frac{\boldsymbol{\tau}}{\rho}\right)\cdot \hat{t}\, ds, \tag{1.2}$$

where $f(y)$ is the Coriolis parameter at latitude y, $\boldsymbol{\tau}$ is the wind-stress vector, ρ is the fluid density and the integral in (1.2) is along the contour C shown in Figure 1. As mentioned above, the contour avoids the region of strong currents on the eastern side of the island.

This particular approximation to the circulation integral to determine ψ_I is called the "Island Rule" and its elegance and simplicity have led to a number of attempts to gauge its validity. The Island Rule yields (Godfrey, 1989) about 12 Sverdrups for the mean meridional transport between Australia and South America, whereas most recent estimates put the observed transport at between 5 and 8 Sverdrups (Wijffels *et al.*, 1996). Indeed, the proximity of Indonesia and neighboring land masses north of Australia makes the neglect of dissipation, topography, and nonlinearity in all of the circuit around the island somewhat problematic. The Island Rule has been extended to attempt to deal with some of these issues by Wajsowicz (1993a,b; 1996). Qui *et al.* (1997) have also used the Island Rule to estimate the wind-driven transport around Hawaii.

In this paper we take up a fundamental study of the general dynamical question of the role of planetary islands in the general circulation. We mean by this, islands large enough so that the β-effect is important. Part of our study is motivated by a desire to re-examine in a fundamental manner the limits of the Island Rule as given by (1.2). That is, how accurate is it when effects of nonlinearity, dissipation, and stratification are non-negligible? It

should be clear from (1.2) that the essence of the rule is a budget for the production of vorticity in the region around and east of the island. In the limit in which (1.2) is valid, the production of planetary vorticity by fluid flowing northward in the region east of the island is given by the (constant) transport times the increase in the planetary vorticity of the fluid as it moves from latitude y_s to latitude y_n. In (1.2) it is balanced by the vorticity put in by the wind. Thus, the issue of the mass transport around the island becomes transformed to a discussion of the vorticity budget of fluid in a zone east of the island. It is thus natural to wonder about the generalization of the Island Rule when nonlinearity, dissipation, and time dependence are no longer negligible. If vortices are shed from the island, or friction on the northern and southern boundaries of the island are important, how is the Island Rule altered? Some of these issues have been raised in the papers already cited but we propose to deal with them in a systematic way by examining the issue with analytical, numerical and laboratory experiments in idealized and controlled situations where the basic dynamical issues can be isolated and studied in detail. Most of our islands are thus of rectangular form, often elongated to represent abyssal ridge systems to which the "island" considerations also apply. The wind-stress system is also of an idealized form, often with a uniform curl over much of the region.

Our interest goes well beyond the quantitative accuracy of the Island Rule prediction of the transport ψ_I. We show below that new physical phenomena arise because of the island and we wish to explore the nature of the physics of the phenomena. In particular, in certain circumstances we find that a robust feature of the dynamics is a recirculation zone, east of the island, that occurs even in linear theory; i.e., when nonlinear advection of momentum and vorticity are neglected. It is of particular interest to follow the character of this recirculation as a function of the Reynolds number of the flow, or equivalently, of the ratio of the western boundary layer's inertial thickness, δ_I, to the viscous Munk layer thickness δ_M, both of which are defined below. At the same time, we explore the role of boundary layers on the northern and southern edges of the island and the role they play in the circulation balance around the island.

Although the Island Rule was originally posed in the context of the wind-driven circulation, the circulation around deep topographic features in the abyss is an area of equally pertinent application of these ideas.

In Section 2 we discuss the general derivation of the Island Rule. This includes effects of nonlinearity, dissipation, and time dependence. We describe generalizations of the Rule to stratified systems although our detailed calculations in this preliminary study are restricted to barotropic models. Of particular interest is the circulation around a meridionally limited ridge where we extend the results of Pedlosky (1994) to include planetary geostrophic effects to show how the recirculation predicted in the earlier theory will "leak" fluid to its surroundings. We also describe the circulation around narrow islands when the orientation of the island is zonal rather than meridional. In preparation for the discussion of the laboratory experiment of Section 3, we discuss the flow around a ridge segment placed meridionally in the sliced cylinder geometry originally studied by Pedlosky and Greenspan (1967).

In Section 3 we present the results of a laboratory experiment which explores the nature of the flow, in particular the predicted recirculation as a function of the ratio δ_I/δ_M; i.e., as a function of increasing nonlinearity. We show first the experimental confirmation of the analytical results when the nonlinearity is moderately small. As the nonlinearity increases new phenomena appear. In particular the nature of the recirculation alters as a separation phenomenon occurs at one extreme tip of the island segment. Section 4 explores the same parameter range with a numerical model and generally good agreement with the experiments is found. Section 5 describes numerical model exploration of other forcings and geometries in order to isolate particular physical phenomena and explore instances of Island Rule violation. Nonlinear features such as eddy shedding and other sources of vorticity fluxes are described along with the critical values of the nonlinearity where important dynamical transitions occur. We also suggest a lower limit for the spacing between the island and the basin boundary in order that the island can be considered truly separated from the outer boundary. In addition, we explore the case of a zonally-elongated island with non-negligible dissipation along its north and south boundaries. In Section 6 we review our results and their implications and describe the direction of future work.

Quite remarkably, although important and interesting alterations of the circulation occur as a result of enhanced dissipation or nonlinearity, the original Island Rule, (1.2), yields, in many cases, quantitatively acceptable estimates for ψ_I in parameter ranges beyond that for which it is formally valid. Thus ψ_I can either be considered a robust feature of the circulation or, equivalently, an insensitive measure of the character of the circulation induced by the presence of the island. Comparisons are also made in terms of the average transport $\overline{\psi}_w$ in the island's western boundary layer, perhaps a better measure of success.

2. Theory

a. Barotropic Island Rule

We begin by deriving the Island Rule for a single layer of homogeneous fluid which satisfies the horizontal momentum equations in the form:

$$\frac{\partial \boldsymbol{u}}{\partial t} + (\zeta + f)\,\hat{k} \times \boldsymbol{u} = -\nabla\left(\frac{p}{\rho} + \frac{|\boldsymbol{u}|^2}{2}\right) + \text{Diss}\,(\boldsymbol{u}) + \boldsymbol{T}, \tag{2.1}$$

where $\hat{k}$ is a vertical unit vector and where $\mathbf{T}$ is the forcing (one can think of it as the wind stress per unit density divided by the fluid depth) and where Diss $(\boldsymbol{u})$ is the representation of the dissipation of horizontal momentum. It could be due to bottom friction or lateral mixing or some combination of the two. The vertical component of the relative vorticity is ζ and f is the Coriolis parameter which we take as a linear function of y; i.e., $f = f_0 + \beta y$. We assume that the motion is horizontally nondivergent and the velocity field is thus derivable from a streamfunction, i.e., $\boldsymbol{u} = \hat{k} \times \nabla\psi$.

When an island exists in an oceanic basin, a fundamental dynamical constraint springs from a consideration of the tangential component of the momentum equation integrated around the island. This yields an equation for the circulation around the island. Since the

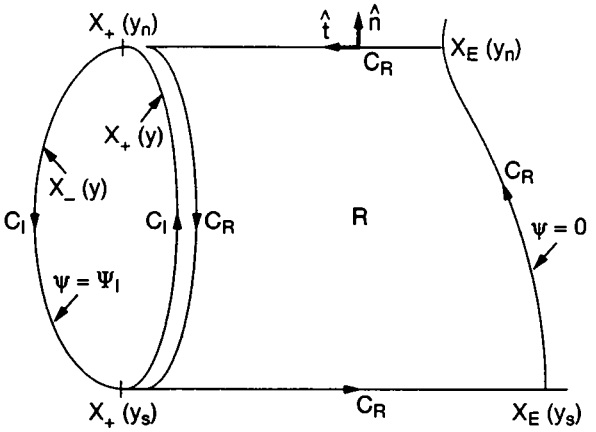

Figure 2. The contours C_I, around the island, and C_R, which runs partly along the eastern boundary of the island. C_R is shown slightly displaced from C for clarity. The two coincide on the island's eastern boundary and run in opposite directions there. The sum of the two contours yield contour C in Figure 1.

velocity normal to the island is zero, the tangential component of the total vortex force [the second term in (2.1)] vanishes on the island. The tangential component of the gradient of the Bernoulli function (the first term on the right-hand side of the equation) is a perfect differential and will vanish when integrated around a closed circuit. Thus integrating in a counter-clockwise circuit, C_I, around the island, we obtain,

$$\frac{\partial}{\partial t}\oint_{C_I} \boldsymbol{u}\cdot\hat{t}\,ds = \oint_{C_I} \boldsymbol{T}\cdot\hat{t}\,ds + \oint_{C_I} \mathrm{Diss}\,(\boldsymbol{u})\cdot\hat{t}\,ds. \tag{2.2}$$

Note that if there is no forcing around the island and if dissipation could be ignored, (2.2) would reduce to the classical condition of conservation of circulation around the island. In that case, the circulation around the island, Γ, and the accompanying value of ψ_I, would need to be specified by initial conditions. This is the traditional situation in potential theory for nonsimply connected regions. In the oceanographic case, we expect to reach at least a statistical steady state under the influence of forcing and dissipation in which, on average, the two terms on the right-hand side of (2.2) must balance.

As mentioned in the introduction, the contour C_I runs along the eastern edge of the island where strong currents and hence substantial dissipation can be expected so that even when friction is generally negligible it must be included over that part of the contour along the eastern edge of the island. We follow the suggestion of Godfrey (1989) and consider the contour C_R which runs along the eastern boundary of the basin between y_s and y_n and then westward along the latitude circle $y = y_n$ until it reaches the island. It then follows the eastern boundary of the island and then returns to the eastern boundary along $y = y_s$ (see Fig. 2). Along this contour the Bernoulli terms also integrate to zero but now the vortex

force tangent to the contour differs from zero on the open boundaries coinciding with the latitude circles y_n and y_s. Thus,

$$\frac{\partial}{\partial t}\oint_{C_R} \boldsymbol{u}\cdot\hat{t}\,ds + \oint_{C_R}(\zeta+f)\,\boldsymbol{u}\cdot\hat{n}\,ds = \oint_{C_R}\boldsymbol{T}\cdot\hat{t}\,ds + \oint_{C_R}\mathrm{Diss}\,(\boldsymbol{u})\cdot\hat{t}\,ds, \tag{2.3}$$

where $\hat{n}$ is the outward unit normal vector to the contour C_R. When we add the integrals (2.2) and (2.3) along the contours C_I and C_R, the portions of the integrals along the eastern boundary of the island cancel since the integrals coincide but run in opposite directions there. The sum of the two contours yields the contour C of Figure 1 which runs around the western portion of the island's perimeter. The integral of the flux of planetary vorticity in (2.3) can be rewritten if we note that the transport between the island and eastern boundary of the basin is independent of latitude for our barotropic incompressible fluid. Thus,

$$\begin{aligned}\oint_C f\boldsymbol{u}\cdot\hat{n}\,ds &= f_n\int_{x_-(y_n)}^{x_e(y_n)} v(x,y_n)\,dx - f_s\int_{x_-(y_s)}^{x_e(y_s)} v(x,y_n)\,dx\\ &= -(f_n-f_s)\psi_I,\end{aligned} \tag{2.4}$$

where $f_n - f_s = \beta(y_n - y_s)$, and we have chosen the streamfunction to be zero on the eastern boundary of the basin and the constant ψ_I on the island. The sum of (2.2) and (2.3) can thus be used to obtain

$$\begin{aligned}\beta(y_n-y_s)\,\psi_I = &-\oint_C \boldsymbol{T}\cdot\hat{t}\,ds - \oint_C \mathrm{Diss}\,(\boldsymbol{u})\cdot\hat{t}\,ds\\ &+\oint_C \boldsymbol{u}\zeta\cdot\hat{n}\,ds + \frac{\partial}{\partial t}\oint_C \boldsymbol{u}\cdot\hat{t}\,ds,\end{aligned} \tag{2.5}$$

where the term involving the flux of relative vorticity differs from zero only along the latitude circles joining the eastern boundary with the northern and southern tips of the island; i.e., it represents the net flux of vorticity out of the region to the east of the island which is girdled by C_R. When dissipation can be ignored in the oceanic interior and on the western boundary of the island, and when nonlinearity is negligible and the circulation has reached a steady state, (2.5) reduces to (1.2). Note that (2.5) could be obtained directly in a single step by integrating the momentum equation directly around the contour C. The approximation (1.2) follows similarly.

There is another useful form of (2.5) that follows from the introduction of the Sverdrup streamfunction $\psi^s(x, y)$. We define the Sverdrup streamfunction as

$$\beta\psi^s = -\int_x^{x_e}\hat{k}\cdot\nabla\times\boldsymbol{T}\,dx', \tag{2.6}$$

in the expectation that it will be a good approximation to the motion in the oceanic interior outside boundary layers on the island or on the basin boundary. We can use (2.6) with Stokes theorem in the simply connected region R, bounded by the contour C_R, to express

the first term in (2.5) as,

$$\begin{aligned}\oint_C \boldsymbol{T}\cdot\hat{t}\,ds &= \oint_{C_I} \boldsymbol{T}\cdot\hat{t}\,ds + \iint_R \beta\frac{\partial\psi^s}{\partial x}\,dx\,dy \\ &= \oint_{C_I} \boldsymbol{T}\cdot\hat{t}\,ds - \beta\int_{y_s}^{y_n}\psi^s(x_+, y)\,dy,\end{aligned} \tag{2.7}$$

where x_+ indicates the value of x at a given y on the eastern portion of the island's perimeter. Thus in the case when dissipation, nonlinearity, and time dependence can be ignored, and when there is no net tangential forcing around the island (so that the first integral on the right-hand side of (2.7) is zero), we obtain from (2.5)

$$\psi_I = \frac{1}{(y_n - y_s)}\int_{y_s}^{y_n}\psi^s\,x_+(y)\,dy, \tag{2.8}$$

so that in this case the constant ψ_I is given by the average value of the Sverdrup streamfunction on the *eastern* side of the island, which is in agreement with the result of Pedlosky (1994).

If we continue the definition of the force $\boldsymbol{T}$ over the area of the island we can define the Sverdrup streamfunction on the western side of the island $x = x_-(y)$ using (2.6). This allows the Island Rule (1.2) to be written as

$$\psi_I = \frac{1}{(y_n - y_s)}\int_{y_s}^{y_n}\psi^s(x_-(y), y)\,dy. \tag{2.9}$$

That is, ψ_I is the y-averaged Sverdrup streamfunction at $x_-(y)$, calculated as though the island were replaced by ocean. When the circulation of $\boldsymbol{T}$ around the island is zero, (2.9) is equivalent to (2.8).

The nonlinear flux of vorticity which enters (2.5) can be written

$$\begin{aligned}\oint_C \boldsymbol{u}\zeta\cdot\hat{n}\,ds &= \int_{x_-(y_n)}^{x_e(y_n)} v\left(\frac{\partial v}{\partial x} - \frac{\partial u}{\partial y}\right)dx - \int_{x_-(y_s)}^{x_e(y_s)} v\left(\frac{\partial v}{\partial x} - \frac{\partial u}{\partial y}\right)dx \\ &= \frac{(v^2-u^2)_{x_e,y_n}}{2} - \frac{(v^2-u^2)_{x_-,y_n}}{2} + \frac{(v^2-u^2)_{x_e,y_s}}{2} - \frac{(v^2-u^2)_{x_-,y_s}}{2} \\ &\quad - \int_{x_-(y_n)}^{x_e(y_n)}\frac{\partial(uv)}{\partial y}\,dx + \int_{x_-(y_s)}^{x_e(y_s)}\frac{\partial(uv)}{\partial y}\,dx.\end{aligned} \tag{2.10}$$

It is natural to imagine that the dominant vorticity flux would occur in the western boundary layer on the eastern side of the island. In that case, and assuming for simplicity that the boundary runs essentially north-south, the boundary layer approximation would allow ζ to be approximated by $\partial v/\partial x$ and the only terms entering the vorticity flux would be the first terms in (2.10) involving $v^2/2$. However, if no-slip conditions hold on all the solid boundaries, this dominant term will vanish as shown by Stewart (1964), and we will be left

with the relatively small terms which form the final line in (2.10). Only when the boundary layer approximation fails, for example when eddies are shed from the end of the island with x and y scales which are comparable, or when eddies are produced in the interior with similar x and y scales, can the vorticity flux terms substantially alter the calculation of ψ_I. Furthermore, the term which remains is the y-derivative of the familiar Reynolds stress and we note that a particular correlation between u and v is necessary for there to be a time-averaged effect on the mean flow. Eddies which contribute to the vorticity flux must "lean" either into or against the shear of the mean for the eddies to contribute to (2.5).

Since the contour C runs around the northern, western and southern portion of the island we expect the dissipation term to be relatively small. However, for islands which have northern and southern boundaries which have a non-negligible length, boundary layers can exist on these boundaries and the dissipation which exists in them cannot be ignored out of hand. These boundary layers, lying along planetary potential vorticity contours are broader than their counterpart on the island's eastern side and the consequently weaker gradients produce less of a frictional force. That force may nevertheless still be important in the calculation of the island streamfunction constant and some of the numerical calculations of Section 5 will reveal circumstances where this is the case. We also give an analytical example below in which the Island Rule is violated as a consequence of the importance of northern and southern boundary layers.

It is straightforward to generalize the above arguments to a stratified fluid and the results are found in the Appendix.

b. Examples

i. Leaky recirculations. Consider the case where the island becomes a long infinitesimally thin ridge segment stretching from y_s to y_n along a meridian at $x = x_t$ in a rectangular basin as shown in Figure 3. We consider the motion to be linear and forced by a pumping of fluid from the upper surface. This may represent either Ekman pumping driven by a wind stress or abyssal motion driven by motion from the abyss into the thermocline. If the north-south scale of the ridge segment is subplanetary the quasi-geostrophic approximation can be used. The horizontal velocity is nondivergent to lowest order in $\beta(y_n - y_s)/f$ and the pressure field acts as a streamfunction. The results of Section 2a will apply directly. In the case when the wind stress is directed zonally there is no tangential component of the forcing acting on the island and we can use (2.8) to determine the constant value of the streamfunction on the island as the meridional average of the Sverdrup streamfunction on the eastern edge of the island.

In the boundary layer on the eastern side of the island the boundary layer transport at each latitude is equal to the difference between the value of the streamfunction on the island and the local value of the Sverdrup streamfunction, ψ^s, at the edge of the boundary layer. Since ψ_I is equal to the average of ψ^s, there must be at least one value of y where they coincide. At the latitude where they coincide, a stagnation point will occur on the island as both the zonal and meridional velocities will vanish there. If ψ^s has a maximum (or

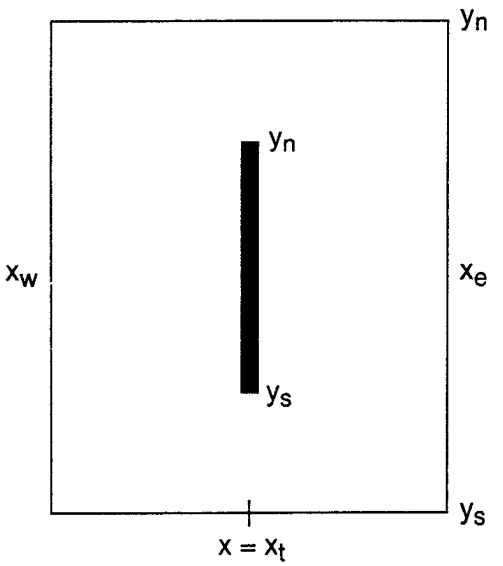

Figure 3. A schematic showing a ridge-like island in an ocean basin. The island is at $x = x_t$ and stretches northward from $y = y_s$ to $y = y_n$.

minimum) along the ridge as is the case if the flow represents a complete gyre, there may be two values of y where $\psi^s = \psi_I$ if the island is long enough in the north-south direction. There will then be two stagnation points. When that occurs a closed region of recirculation is predicted. It is not hard to show that the recirculation will form a gyre lying to the east of the island as in Figure 4, provided $|\psi^s|$ reaches a maximum within the latitude band of the island. (If $|\psi^s|$ reaches a single minimum, the stagnation streamlines will wrap around to the west of the island and a more complicated picture will emerge.) This zone is formed by the interior streamline which joins the two stagnation points and, of course, the value of the streamfunction on this bounding line is simply ψ_I. This result is discussed in Pedlosky (1994) using a linear model and an example of such a circulation is shown in Figure 4. The recirculation is an entirely linear phenomenon; its shape and structure are defined by the Sverdrup streamfunction and the stagnation points as determined by the Island Rule.

A little reflection reveals, though, that this cannot be the whole story. In the domain of the recirculation, i.e., in the region between the island and the streamline $\psi^s = \psi_I$, fluid pumped down from the Ekman layer (for the wind-driven problem) will add to the fluid contained in the recirculation zone. (Similar considerations hold for a model of the abyssal flow where fluid leaves the abyss and is drawn into the thermocline.) Were the recirculation truly isolated, the mass of the region would continuously increase with time as fluid enters the isolated region and this is of course impossible for an incompressible fluid. The resolution of this difficulty is rather simple. The volume of fluid pumped down from the Ekman layer is $O(\beta(y_n - y_s)/f)$ smaller with respect to the flux of the horizontal circulation. This is the basis of the β-plane approximation and the quasi-geostrophic theory

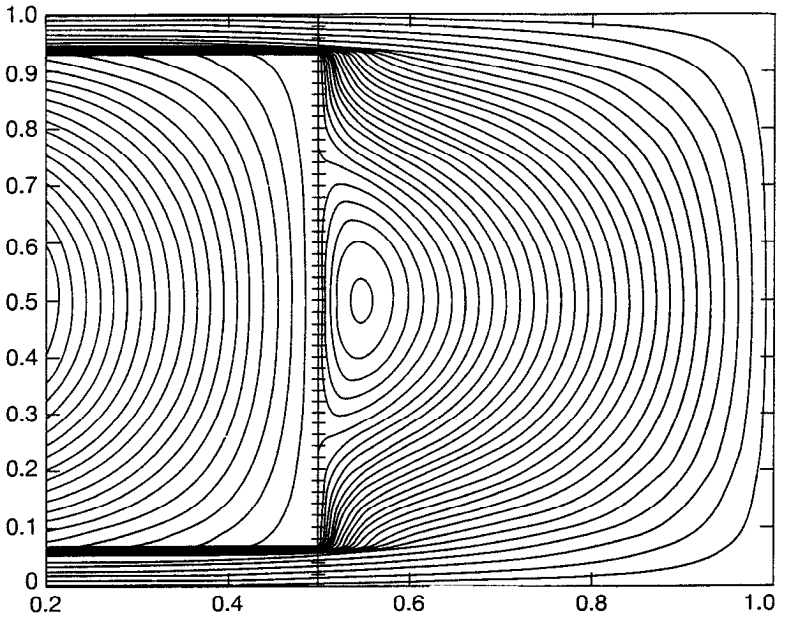

Figure 4. The recirculation according to quasi-geostrophic theory. The island is a meridional barrier which interrupts a Sverdrup gyre. The stagnation points are determined by the Island Rule.

in which the Ekman pumping acts, through the stretching of planetary vorticity filaments, as a vorticity source while the mass flux associated with the Ekman pumping is ignored. It is necessary to include planetary geostrophic effects; i.e., to go beyond quasi-geostrophic theory, that is, to include the explicit variation of f throughout the calculation in order to describe the complete mass flux balance. These higher-order effects produce a "leak" in the recirculation zone. As an illustration we consider the linear limit of the flow where nonlinearity can be neglected and where the dissipation is modeled by lateral friction alone. Thus the governing equations are,

$$fu = -\frac{\partial P}{\partial y} + A\nabla^2 v,$$

$$-fv = -\frac{\partial P}{\partial x} + A\nabla^2 u, \qquad (2.11\text{a,b,c})$$

$$\frac{\partial u}{\partial x} + \frac{\partial v}{\partial y} = -\frac{w_e}{D},$$

where A is the coefficient of viscosity (or turbulent mixing of momentum), P is the pressure divided by the density, D is the thickness of the layer and w_e is the velocity imposed at the upper surface. For weak dissipation the motion will be in geostrophic balance outside boundary layers on the island and the basin's western boundary. The interior solution is

determined geostrophically entirely by the pressure field, P_s. In the region east of the island the solution is the Sverdrup solution:

$$P_s = -\frac{f^2}{\beta}\int_x^{x_e} \frac{w_e}{D}\, dx'. \tag{2.12}$$

In the boundary layer on the eastern side of the island the meridional velocity can be shown to remain in geostrophic balance although this is not true for the zonal velocity. If we write the pressure and velocities as a sum of the interior solution plus a correction, e.g.,

$$P = P_s + \tilde{P}, \tag{2.13}$$

it is possible to show that to lowest order,

$$\begin{aligned} f\tilde{v} &= \frac{\partial \tilde{P}}{\partial x}, \\ f\tilde{u} &= -\frac{\partial \tilde{P}}{\partial y} + A\frac{\partial^2 \tilde{v}}{\partial x^2}, \\ \frac{\partial \tilde{u}}{\partial x} &+ \frac{\partial \tilde{v}}{\partial y} = 0. \end{aligned} \tag{2.14a,b,c}$$

The pressure correction satisfies the Munk boundary layer equation. The total solution can thus be written,

$$\begin{aligned} P &= P_s(x, y) + B(y)F(\xi), \\ F(\xi) &= e^{-\xi/2}\left[\cos\frac{\sqrt{3}\xi}{2} + \frac{1}{\sqrt{3}}\sin\frac{\sqrt{3}\xi}{2}\right], \\ \xi &= (x - x_t)/\delta_M, \end{aligned} \tag{2.15a,b,c}$$

where the Munk layer thickness

$$\delta_M = \left(\frac{A}{\beta}\right)^{1/3}, \tag{2.16}$$

and where $B(y)$ is an arbitrary function of y.

The form of $F(\xi)$ already satisfies the condition of no-slip on the island's eastern boundary. However to satisfy the no-zonal flow condition there, (2.14b) must be used. This leads to an ordinary differential equation for $B(y)$,

$$\frac{dB/f}{dy} = -\frac{1}{f}\frac{\partial P_s(x_t, y)}{\partial y}, \tag{2.17}$$

which when integrated yields

$$B = -P_s(x_t, y) - f\int_{y_0}^{y} \frac{\beta}{f^2} P_s(x_t, y')\, dy' + \frac{f}{f_0} B_0, \tag{2.18}$$

where B_0 is an integration constant and y_0 is arbitrary. *The Island Rule no longer holds in its original form since the motion under consideration is now horizontally divergent.* It is necessary to return to the original constraint (2.2). Since there is no forcing tangent to the island, and since the major dissipation exists in the boundary layer on the eastern side of the island, the constraint reduces to the condition that the integral along the island's length of the frictional force $A\partial^2 v/\partial x^2$ on the eastern side must vanish. This determines B_0 and the solution in this region east of the island is

$$P = P_s(x, y) + F(\xi)\left[-P_s(x_t, y) + \frac{f_n}{\Delta f}\int_{y}^{y_n} \frac{\beta}{f^2} P_s(x_t, y')\, dy' + \frac{f_s}{\Delta f}\int_{y_s}^{y} \frac{\beta}{f^2} P_s(x_t, y')\, dy'\right], \tag{2.19}$$

where $\Delta f = f_n - f_s$. In the quasi-geostrophic limit the factor β/f^2 can be treated as a constant in the two integrals and the square bracket reduces, in that case, to the difference between P_s and its average along the island's meridional extent, as given by the Island Rule. This means, in particular, that the coefficient, $B(y)$, of $F(\xi)$ will always, in the quasi-geostrophic limit, vanish at the same value of P_s, that is, the stagnation points will be joined by the same interior isoline of pressure, isolating the recirculation region at lowest order in the quasi-geostrophic limit. Instead, it is clear from (2.19) that the zeros of the square bracket will now occur at different values of P_s. It is not difficult to show, and it is left as an exercise for the reader, that when P_s is positive, representing an anticyclonic Sverdrup circulation, the northern stagnation point occurs at a lower value of P_s than the southern stagnation point. This leads to the configuration of flow shown in Figure 5. The isoline $P_s = P_1$ lies everywhere east of the isoline $P_s = P_2$. Fluid pumped into the recirculation region spirals anticyclonically and moves northward until it reaches the stagnation point at $y = y_1$ on $P_s = P_1$. It flows southward and when it enters the boundary layer it finds itself south of the southern stagnation point at $y = y_2$. In this region the boundary layer flow is southward and the fluid escapes from the recirculation zone. It is also not difficult to show that the fluid crossing the P_1 isoline in the boundary layer is exactly equal to the fluid pumped out of the Ekman layer within the area bounded by the P_1 isoline and the ridge segment which perfectly accounts for the mass balance. If the forcing is reversed so that fluid is forced up into the Ekman layer the linear theory predicts only a reversal of flow direction. The flow then enters the recirculation zone from the south and spirals inward to be sucked up into the upper Ekman layer. The topology of the circuit is the

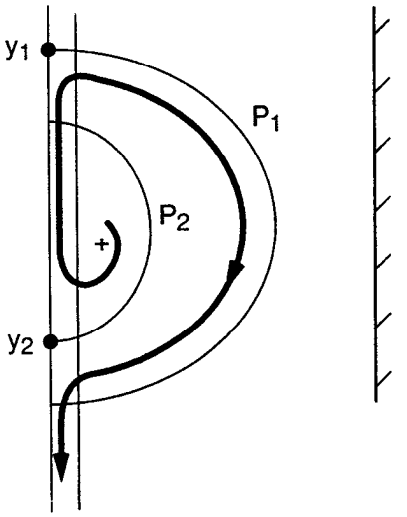

Figure 5. A schematic showing the stagnation points and the leaky recirculation for the case of Ekman pumping and anticyclonic Sverdrup flow. The displacement of the stagnation points from the same interior isobar allows fluid to leak southward out of the recirculation zone in the western boundary layer.

same and the penetration of the recirculation zone by external fluid remains in the southern part of the recirculation flow.

The leak is relatively small; i.e., $O(\beta(y_n - y_s)/f)$ compared to the quasi-geostrophic circulation driven by the vorticity compression of the Ekman pumping and so the residence time of fluid in the region of recirculation is longer than the exterior advective time by the inverse of this factor. However, its presence is easily observable in the experiments reported on in Section 3 and it also represents a phenomenon not derivable from the Island Rule.

ii. The sliced cylinder. The sliced-cylinder was introduced by Pedlosky and Greenspan (1967) as a simple laboratory analog for the oceanic circulation. The cylinder, of maximum depth D and radius r_0, spins on its axis and is forced by differentially rotating its upper surface at a rate $\Delta\Omega$ with respect to the rotation of the cylinder's side wall. The bottom of the cylinder is sloped linearly so that the depth decreases across a diameter of the cylinder by an amount ΔD. The slope

$$s = \frac{\Delta D}{(2r_0)} \tag{2.20}$$

yields an equivalent β-effect

$$\beta_{eq} = \frac{fs}{D}. \tag{2.21}$$

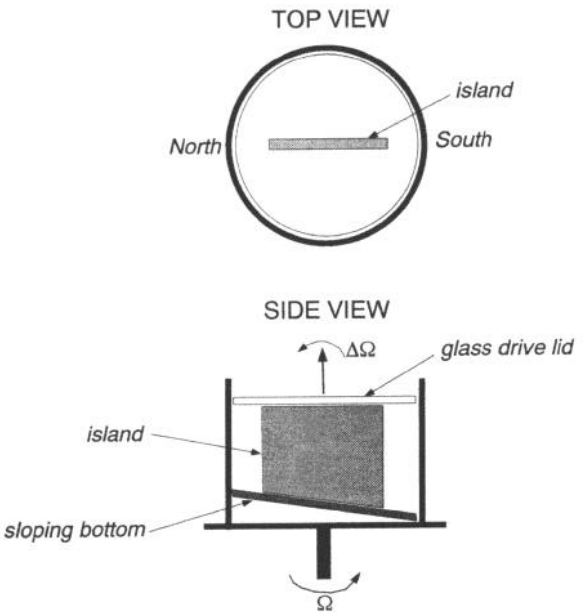

Figure 6. The configuration of the sliced-cylinder experiment with the ridge segment forming an island barrier.

The differential rotation of the upper lid of the cylinder gives rise, in the case of anticyclonic forcing, to an Ekman downwelling into the interior of the cylinder which is spatially uniform and equal to:

$$w_e = \left(\frac{2\nu}{f}\right)^{1/2} \Delta\Omega, \tag{2.22}$$

where ν is the kinematic viscosity of the fluid.

The linear quasi-geostrophic solution for the resulting flow is very similar to the one found in the previous example and we do not give the details of the solution. We place a ridge-like barrier running south to north along the cylinder's diameter leaving small gaps at the northern and southern ends as shown in Figure 6.

East of the island the interior Sverdrup solution is:

$$\psi^s = \frac{T}{\beta_{eq}}[x - \sqrt{r_0^2 - y^2}], \tag{2.23}$$

where $T = fw_e/D$. In the quasi-geostrophic limit, variations of D are ignored unless D is differentiated. Note that the curvature of the interior streamlines, necessary for the production of the recirculation region, is due entirely to the curvature of the "eastern" boundary of the cylinder since the Ekman pumping is spatially uniform. The boundary layer on both the ridge and the western boundary of the cylinder is the classical Munk layer.

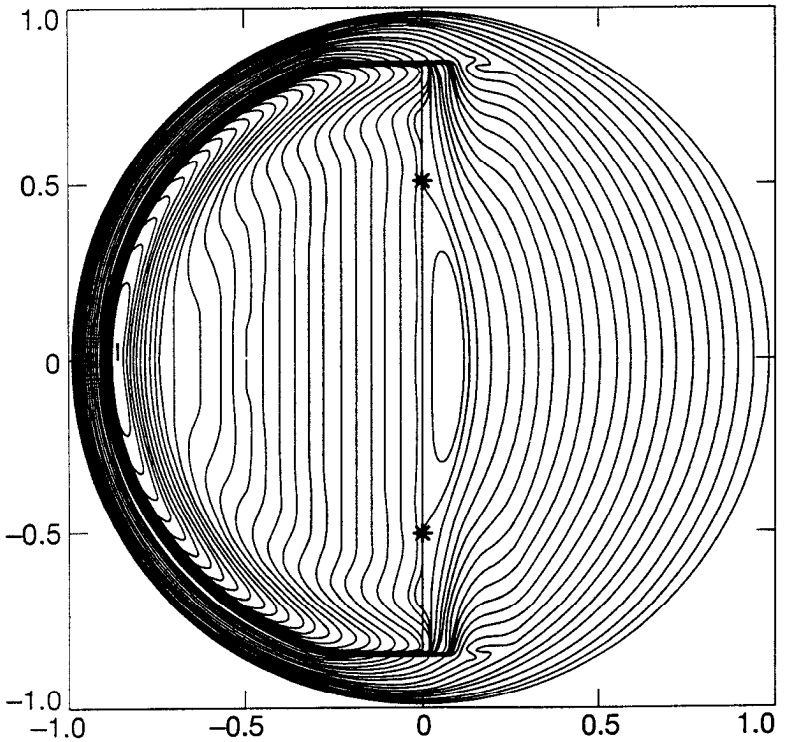

Figure 7. The linear, quasi-geostrophic boundary solution, using boundary layer methods, obtained for the sliced cylinder. In the example shown, $\delta_M/r_0 = .0394$ and the distance between the tip of the ridge and the cylinder is $0.15r_0$. The value of $\psi_I = -0.861$. The stagnation points are at $y/r_0 = \pm 0.586r_0$, while the maximum eastward extent of the recirculation region is $0.14r_0$. The solution is constructed by boundary layer methods and the unrealistic projection of the boundary layer to the east of the ridge at its terminal points is an artifact of the boundary layer solution.

On the ridge the constant value of the streamfunction can be found, in the quasi-geostrophic approximation, by the Island Rule, most conveniently in the form (2.8).

This leads to

$$\psi_I = \frac{-T}{2\beta_{eq}(y_n - y_s)} \left\{ \begin{array}{l} y_n\sqrt{r_0^2 - y_n^2} - y_s\sqrt{r_0^2 - y_s^2} \\ \quad + r_0^2\left(\sin^{-1}\left(\dfrac{y_n}{r_0}\right) - \sin^{-1}\left(\dfrac{y_s}{r_0}\right)\right) \end{array} \right\}. \tag{2.24}$$

With the constant on the island determined, the stagnation points are easily found and the extent of the recirculation region can be predicted. Figure 7 shows an analytical, quasi-geostrophic calculation of the resulting circulation. The region of trapped fluid extends about 15% of the cylinder's radius at its maximum eastward point. Only about 10% of the circulation which would pass from the western to eastern sub-basin is blocked by the island (This is equal to the amount trapped in the recirculation region.) The rest

works its way through the narrow gaps (here each 15% of the radius) to flow around the sac of recirculation. Note that to the west of the island the streamlines run parallel to the island-ridge in the interior since the Ekman pumping is spatially uniform. Only in the vicinity of the western boundary layer do the streamlines bend from lines of constant x.

The leak from the recirculation zone can also be calculated precisely in the manner of the previous section. Instead of the variation of f that must be taken into account, now the variation of D itself must be considered. The result is qualitatively similar and not reproduced here. The recirculation is predicted to leak from the south at a rate of $O(sr_0/D)$ with respect to the flow forced by the vortex compression due to the Ekman pumping. Again, the residence time of fluid in the sac of recirculation will be longer than the time taken by fluid external to the sac to traverse the scale of the basin by the inverse of this factor.

Bottom friction, i.e., the consequences of the bottom Ekman layer have not been included in the calculation of the boundary layer. However, according to the Island Rule, which is valid in this low-friction limit, the value of ψ_I and hence the position of the stagnation points and the extent of the recirculation is independent of the details of the dissipation mechanism.

The inertial boundary layer width is defined as (Pedlosky, 1987)

$$\delta_I = \left(\frac{U_s}{\beta}\right)^{1/2} \tag{2.25}$$

where U_s is a typical value of the interior Sverdrup flow. In the present case one can estimate U_s as

$$U_s = \left(\frac{2\nu}{f}\right)^{1/2} \frac{\Delta\Omega}{s}. \tag{2.26}$$

Thus, the measure of nonlinearity, given by the ratio of δ_I/δ_M is

$$\frac{\delta_I}{\delta_M} = \frac{2^{1/3} R_0^{1/2}}{E^{1/12} s^{2/3}} \tag{2.27}$$

where

$$R_0 = \frac{\Delta\Omega}{2\Omega}, \qquad E = \frac{\nu}{\Omega D^2}. \tag{2.28}$$

The solution shown in Figure 7 is formally valid in the limit when the ratio in (2.27) goes to zero, but we will show below that qualitatively, the solution is a good predictor of the structure of the flow for moderate values of δ_I/δ_M.

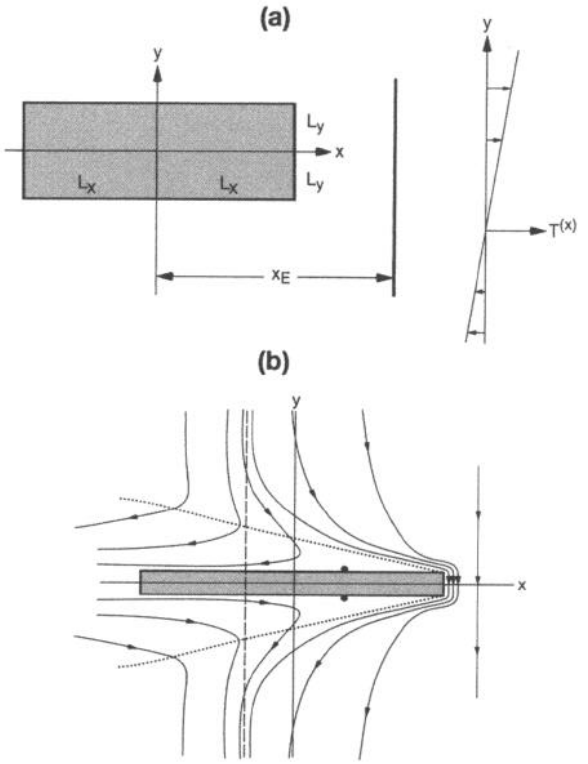

Figure 8. (a) A rectangular island centered at $x = 0$, $y = 0$, with a total east-west length $2L_x$ and a total north-south length $2L_y$, the center of the island is at a distance x_e from the eastern boundary. The flow around the island is driven by a zonal wind stress with a constant curl. (b) A schematic of the circulation in the limit when the island shrinks to a zonal ridge. The points with a heavy dot are the stagnation points. The dashed line indicates the longitude where the zonal transport in the boundary layers changes sign.

iii. Zonally oriented island. The Island Rule in its original form (1.2) assumes that friction is negligible except on the eastern side of the island where the strongest boundary currents are. If the island has northern and southern boundaries which parallel planetary vorticity isolines, diffusive boundary layers exist on those boundaries. These layers are broader than the layer on the eastern boundary of the island and hence the contribution to the dissipation term in the extended Island Rule (2.5) will be asymptotically small when, all other things being equal, the friction is limited to the boundary layers. However, if the island's east-west length exceeds its north-south length, the dissipation on the northern and southern boundaries may become as large as that on the eastern boundary and the Island Rule may fail in its original form. The interesting limiting case is a narrow island or abyssal ridge, as discussed in the previous examples, although now oriented in an east-west direction. The general configuration before the limit is taken is shown in Figure 8a.

For simplicity, consider the quasi-geostrophic, linear model in which the dissipation is modeled as a bottom friction; i.e., Stommel's model. We let the flow be driven by a constant wind-stress curl with the wind stress zonal and a linearly increasing function of y. The vorticity equation becomes,

$$\frac{\partial \psi}{\partial x} = \frac{1}{\beta} W - \delta_s \nabla^2 \psi \tag{2.29}$$

where

$$W = \hat{k} \cdot \nabla \times \boldsymbol{T}, \qquad \delta_s = \frac{r}{\beta}, \tag{2.30}$$

and r is the inverse of the spin-down time due to bottom friction.

We approach the solution by boundary layer methods assuming that δ_s is small compared to L_x, the half-width of the island. There are three boundary layers. There is, of course, one on the eastern side of the island which has the structure of the standard Stommel boundary layer with thickness δ_s. Note that it does not enter explicitly in the Island Rule calculation (2.6) for the value of the streamfunction on the island since the contour C avoids the island's eastern boundary entirely.

On the northern and southern boundary of the island there are boundary layers whose widths in the y-direction are of order $(\delta_s L_x)^{1/2}$. If we write the total solution as the sum of the Sverdrup streamfunction, ψ^s, and a correction function ϕ, where,

$$\psi^s = (x - x_e) \frac{W}{\beta}, \tag{2.31}$$

and where the correction function $\phi(x, y)$ vanishes outside the boundary layer, it is possible to show that ϕ, to lowest order, satisfies the diffusion equation,

$$\frac{\partial \phi}{\partial t} = \delta_s \frac{\partial^2 \phi}{\partial y^2}, \tag{2.32}$$

where $t = L_x - x$. The boundary layer is infinitesimally thin on the eastern edge of the island and grows parabolically westward in the direction of increasing t. It is important to note that this westward thickening is independent of the direction of flow in the layer since the problem is linear and advection of relative vorticity does not enter the physics. The diffusive character of the boundary layer is due to the coincidence of the boundary with a potential vorticity contour. Similar boundary layers were first discussed by Pedlosky (1968, 1974) and Csanady (1978).

On the northern boundary the total streamfunction must equal the island constant ψ_I which means that

$$\phi = \psi_I - \psi^s(x, L_y) \qquad \text{on} \qquad y = L_y, \tag{2.33}$$

while for all $y > L_y$, $\phi = 0$ at $t = 0$ (i.e., at the initiation of the boundary layer where it merges with the interior).

The solution which satisfies (2.32) and the boundary conditions is easily found,

$$\phi = \left[\psi_I - \frac{W}{\beta}(L_x - x_e)\right] Erfc\left(\frac{\eta}{2t^{1/2}}\right) + \frac{W}{\beta}\left[\left(t + \frac{1}{2}\eta^2\right) Erfc\left(\frac{\eta}{2t^{1/2}}\right) - \frac{\eta t^{1/2}}{\sqrt{\pi}} e^{-(\eta^2/4t)}\right] \tag{2.34}$$

where $\eta \equiv (y - L_y)/\delta_s^{1/2}$ is the stretched boundary layer variable. $Erfc\,(x)$ is the complementary error function. The boundary layer on $y = -L_y$ is similar. With (2.34) and the similar solution on $y = -L_y$, it is possible to now carry out explicitly the integrals indicated in the extended Island Rule (2.5). Neglecting nonlinearity and recalling that the curl of the stress is a constant over the basin, we obtain

$$\beta\psi_I\left\{(y_n - y_s) + 4\sqrt{\frac{2}{\pi}}(\delta_s L_x)^{1/2}\right\} = W\left[-((L_x + x_e)(y_n - y_s)) + \sqrt{\frac{2}{\pi}}(\delta_s L_x)^{1/2}\left(4(L_x - x_e) - \left(\frac{16L_x}{3}\right)\right)\right], \tag{2.35}$$

where $y_n - y_s = 2L_y$.

The first term in each large bracket is what the Island Rule would yield in the absence of the consideration of the boundary layer contributions from the northern and southern boundaries of the island. Indeed these latter terms are negligible as long as

$$\frac{L_y}{(\delta_s L_x)^{1/2}} \gg 1. \tag{2.36}$$

If the island width L_y is larger than the boundary-layer thickness $(\delta_s L_x)^{1/2}$ then the contributions from the northern and southern boundary layers will be negligible in the same parameter range ($\delta_s \ll L_x$) for which standard boundary layer theory applies. However, if we let the north-south scale of the island shrink until the inequality in (2.36) is reversed, the contributions from the northern and southern boundary layers become the dominant contributors to the extended Island Rule in which case, in this limit

$$\psi_I = \frac{W}{\beta}\left[L_x - x_e - \frac{4}{3}L_x\right], \quad \frac{L_y}{L_x} \ll \left[\frac{\delta_s}{L_x}\right]^{1/2} = -\frac{W}{\beta}\left[\frac{L_x}{3} + x_e\right], \tag{2.37}$$

which is quantitatively quite different than the Island Rule prediction. Note that if we had neglected the contributions from the northern and southern boundary layers, the Island

Rule would consist of two terms, each going to zero as $y_n - y_s$ goes to zero and yielding as a limit,

$$\psi_I^{\text{Island Rule}} = -\frac{W}{\beta}(L_x + x_e). \tag{2.38}$$

The circulation predicted in this limit is rather unexpected and is shown schematically in Figure 8b for the case of the zonally oriented ridge/island. First of all, the western boundary layer survives in the limit of vanishing north-south width of the island. The island continues to recognize its eastern boundary as a conduit for mass around the island even as the length of this boundary shrinks to zero. The transport in this boundary layer is equal to the difference between the Sverdrup streamfunction at the eastern tip of the island and ψ_I as given by (2.37). The flux that passes through the boundary layer on the island's eastern tip is thus

$$\psi^s(L_x, 0) - \psi_I = \frac{W}{\beta}\left(\frac{4}{3}L_x\right). \tag{2.39}$$

In the case when $W < 0$ this mass flux is southward and fed from the northern boundary layer. The flow makes a 180° U-turn at the eastern edge of the ridge and flows westward in the southern boundary layer and feeds the interior Sverdrup flow to the south of the island. Stagnation points exist on both northern and southern sides of the island, at the same x-position, at the point where the y-derivative of ϕ vanishes. These points, where u and v vanish on the island, occur at $x = L_x/3$ on each side of the island. It is important to note, however, that the zonal *transport* in the boundary layer vanishes at $x = -L_x/3$ as can be shown from (2.34) and (2.37). Indeed, at the stagnation point the zonal boundary-layer transport is $-(W/\beta)(2L_x/3)$. That, supplemented by the entrainment of the Sverdrup transport which occurs between the stagnation point and the eastern tip of the island $(-(W/\beta)(2L_x/3))$ yields the transport in the western boundary current given by (2.39). The flow to the west of the stagnation point cannot close in a boundary layer on the western side of the island. Instead, for very small friction, it flows to the western boundary of the basin, makes a U-turn there and flows back to the southern side of the island to complete the circulation as shown in Figure 8b. It is clearly a very strange and unrealistic circulation that linear theory predicts. It is hard to accept that a fluid, even at low Rossby number, can succeed in making the hairpin turns that linear theory demands without separating from the island's edge. We will take up the nonlinear problem in Section 4 to examine the question further.

Figure 9, which anticipates some of the discussion of Section 4, shows a numerical calculation in the linear regime for the case where the dissipation is due to bottom friction. The inertia, though small, is not completely negligible in the calculation. That is, the ratio $\delta_I/\delta_s = 0.125$. We see, though, that the qualitative predictions of linear theory are amply supported in the calculation. There is a stagnation point on each surface located at $x =$

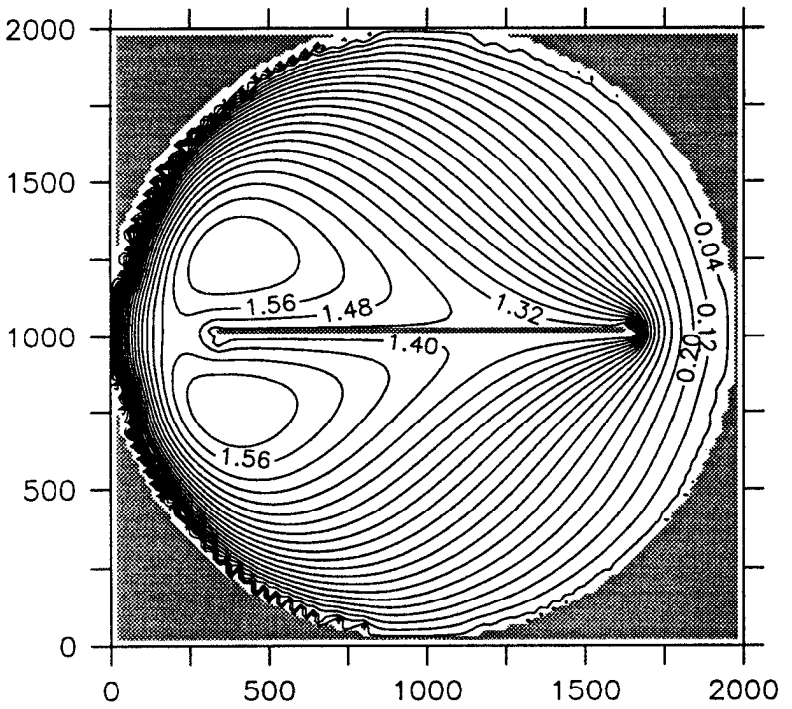

Figure 9. The flow around a ridge-shaped island oriented in the zonal direction embedded in a circular basin. The dissipation is due to bottom friction, and the wind stress curl is spatially uniform. The ratio $\delta_I/\delta_s = 0.125$. Note the hairpin turn the flow takes around the eastern tip of the island. In this limit the Island Rule is invalid.

$.34L_x$, in close agreement with theory. The flow to the east of it flows around the eastern tip of the island making the U-turn predicted by boundary layer theory! The friction is large enough so that the trailing jets to the west of the island diffuse sufficiently to merge smoothly into the Sverdrup flow in the interior west of the island. In Section 4 we follow the evolution of similar flows with lateral friction as the ratio δ_I/δ_M increases. We would like to emphasize, even before considering the change in the phenomenology that occurs when the flow becomes nonlinear, that the Island Rule (1.2) is quantitatively invalid in this case even in the linear regime due to the dominance of dissipative effects on the northern and southern boundaries of the island.

If instead of using bottom friction we use lateral friction, the problem turns out to be structurally very similar with only quantitative differences. These quantitative differences are, however, significant for the dependence on the details of the dissipation implies the breakdown of the Island Rule in the limit of small $L_y/\delta_M^{3/4}L_x^{1/4}$ (the ratio of the island width to diffusive boundary-layer thickness). For lateral friction, the point where the zonal transport reverses occurs at $x = -(3L_x/5)$ slightly westward of the bottom friction case, and the flow in the boundary layer on the eastern side of the island is now $8WL_x/5\beta$. Now ψ_I is, in this

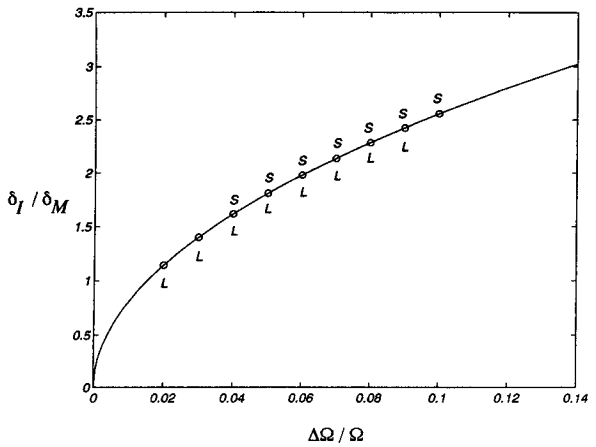

Figure 10. δ_I/δ_M versus $\Delta\Omega/\Omega$, (2.27), with the values examined in the experiments indicated by circles. The figure also shows the flow regimes observed in the experiments. The letter L indicates that the linear recirculation was observed and the S identifies the presence of flow separation at the northern end of the island.

case, given by

$$\psi_I = -\frac{W}{\beta}\left[\frac{3L_x}{5} + x_e\right] \qquad \text{(lateral friction)}, \tag{2.40}$$

instead of (2.37), a small quantitative difference.

3. The experiment

a. Method

The experimental configuration shown in Figure 6 is a variation on the classic rotating sliced cylinder experiment (Pedlosky and Greenspan, 1967). The tank is a Plexiglas cylinder with internal radius $r_0 = 16.75$ cm fitted with a uniformly sloping bottom, $s = 0.15$. The island is a 1.27-cm-thick Plexiglas sheet that occupies the full depth of the water column and extends $0.85r_0$ from the center of the tank toward the shallowest and deepest parts. This gives a meridionally oriented island in the topographic equivalent of the β-plane. The flow is driven by a glass plate that is differentially rotated at rate $\Delta\Omega$ relative to the basic counterclockwise tank rotation of $\Omega = 2\ \text{s}^{-1}$. The plate is supported around its perimeter to allow visualization of the center of the tank and is driven by a drive belt connected to a geared stepper motor. The working fluid is water ($\nu = 0.01\ \text{cm}^2\ \text{s}^{-1}$) with a mean depth $D = 20$ cm.

For all the experiments reported here the experimental parameters Ω, D, ν, and s were held at the values listed above fixing $E = 1.25 \times 10^{-5}$ and $\delta_M = 0.69$ cm. The flow dependence upon δ_I/δ_M (2.27) was explored by varying $\Delta\Omega$. In all runs $\Delta\Omega$ was negative giving Ekman downwelling and anticyclonic interior circulation. Figure 10 shows a plot of

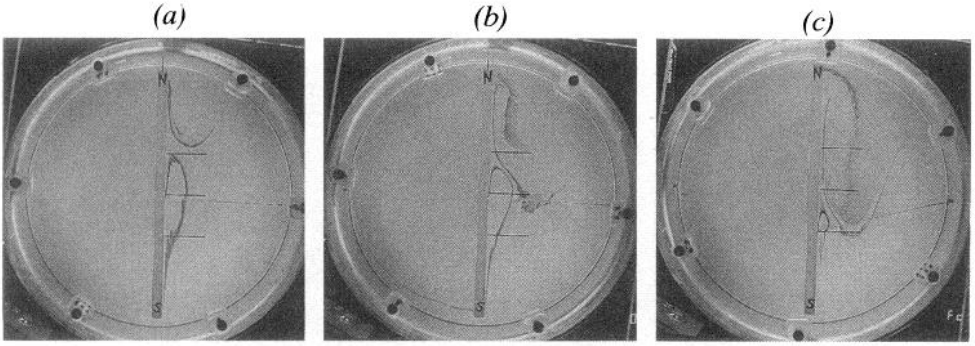

Figure 11. Photographs of several experimental runs with the thin meridional ridge illustrating the effects of increasing nonlinearity. In the figures the equivalent north is to the top of the images and the extent of the island is indicated by the markings N and S. Note that the north-south extent of the island is exaggerated by parallax effects. Dye is slowly introduced at mid-depth at two locations: the northern edge of the island and at a point along the eastern side of the island. (a) $\delta_I/\delta_M = 1.42$, (b) 1.83, (c) 2.45.

δ_I/δ_M versus $\Delta\Omega/\Omega$ with symbols indicating the values of δ_I/δ_M investigated in the experiments. We were unable to achieve values of δ_I/δ_M less than about 1.14 because of unsteady disk rotation rates at these very low speeds.

The flow was visualized by pumping dye through syringes positioned at two locations in the tank. The first was along the northern end of the island at the mid-depth of the fluid. This dye marked fluid entering the eastern sub-basin and indicated any flow separation at that end of the island. The second injection was along the eastern side of the island at mid-depth. The north-south location varied between runs. This second injection marks (nearly) the streamline separating the recirculation zone from the Sverdrup interior. Both injections were at very low rates, about 1 cm^3/hr, and contributed negligible mass flux into the system. Measurements of meridional velocity profiles and transports in the eastern basin were obtained using the thymol blue indicator technique. The cathode for marking the fluid was positioned at mid-depth and ran from the center of the island directly east to the basin boundary (along $y = 0$). The experiments were recorded on video tape and 35-mm film.

b. Results

Figure 11a shows a photograph of an experimental run at $\delta_I/\delta_M = 1.42$. Dye released at the center of the island proceeds northward along the island boundary until nearing the stagnation point. It then turns southeastward into the interior to define the recirculation zone. The dye leaks out of the recirculation zone at the southern end to eventually return to the western sub-basin in agreement with the mass flux constraint discussed in Section 2. The dye released at the northern edge of the island proceeds directly south after turning the corner with no indication of flow separation. Note that the leading edge of this northern dye streak appears to be heading to the northeast. However, the flow is to the south and the dye

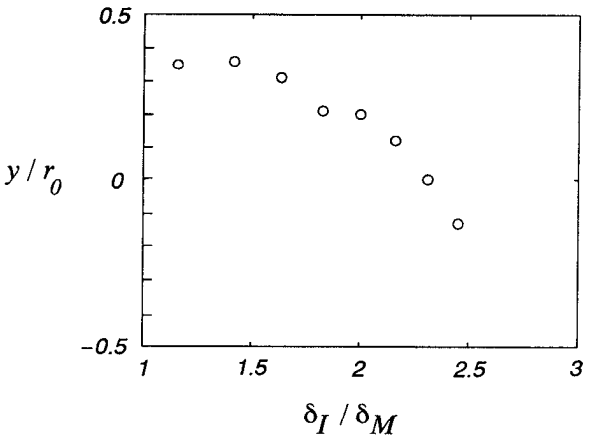

Figure 12. The northern limit of the dye in the linear recirculation zone y/r_0 versus δ_I/δ_M.

pattern is the result of passive advection of a finite size patch of dye resulting from the initiation of the injection. The flow is steady. The value $\delta_I/\delta_M = 1.42$ is in the nonlinear regime, but the observed circulation on the eastern side of the island agrees qualitatively with the linear solution shown in Figure 7.

As the nonlinearity of the flow is increased, a significant change in the flow pattern occurs. Figure 11b shows a run with $\delta_I/\delta_M = 1.83$. The recirculation zone is still present, but now shifted to the south with a more prominent north-south asymmetry. Dye released at the northern edge of the island separated from the island before turning south into the interior. This separation results in a second, northern, recirculation cell which extends from the tip of the island to the northern edge of the linear recirculation cell. The flow is still steady. Figure 11c shows an experiment at $\delta_I/\delta_M = 2.45$. The southern linear recirculation has now moved to the southern half of the island and is very small. The northern separation recirculation extends meridionally more than one-half of the island length. Further increase of the nonlinearity eliminates the linear recirculation and introduces weak unsteadiness in the flow, but the northern recirculation bubble remains.

The observed flow pattern as a function of δ_I/δ_M is summarized in Figure 10. For $\delta_I/\delta_M < 1.5$ there is no flow separation and the recirculation zone agrees qualitatively with the linear theory. For $1.5 < \delta_I/\delta_M < 2.5$, the flow separates from the northern edge of the island and two recirculation zones appear. For $\delta_I/\delta_M > 2.5$, the linear Island Rule recirculation zone is eliminated while the separation recirculation remains.

Figure 12 shows the northern limit of the dye in the linear recirculation zone. For $\delta_I/\delta_M < 1.5$, the dye reaches to about $y = 0.35r_0$. This is less than the theoretical stagnation point location of $y = 0.51r_0$ from (2.23) and (2.24). When the finite width of the island is accounted for, the theoretical stagnation point moves to $y = 0.47r_0$, and $y = 0.45r_0$ when the asymmetry of the recirculation due to the Ekman flux is considered. The remaining discrepancy between the experiment and the theory is probably due to the fact that the dye

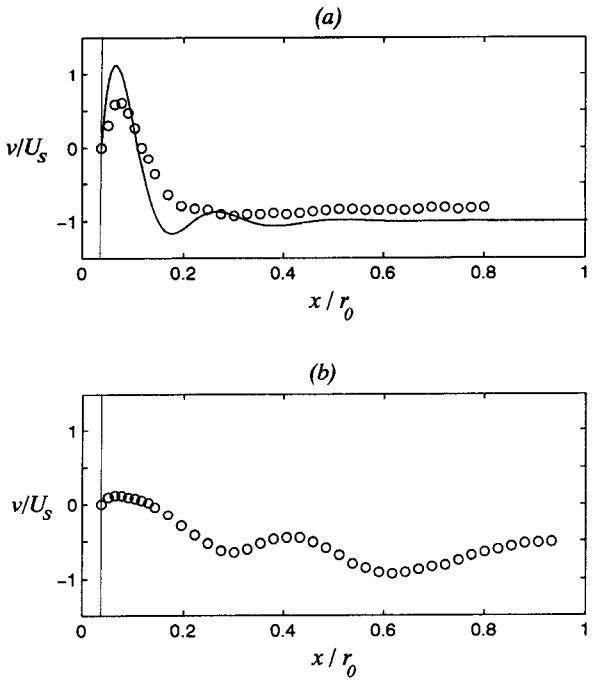

Figure 13. Meridional velocity profiles to the east of the island along $y = 0$. (a) $\delta_I/\delta_M = 1.42$, (b) $\delta_I/\delta_M = 2.14$. The measured velocities are indicated by the circles and in (a) the solid line is the linear theory. The velocities are normalized by U_s (2.26). The vertical line at $x/r_0 = 0.038$ indicates the eastern side of the island.

gives an underestimate of the stagnation point location. It would take a very long time for dye to reach the stagnation point due to the very low velocities near the point. The zonal extent of the recirculation is $0.15r_0$ for $\Delta_I/\delta_M < 1.5$, in good agreement with the theory. As δ_I/δ_M is increased above 1.5, the northern limit of the recirculation moves south. This point also indicates the southern limit of the separation recirculation zone.

Figure 13 shows two meridional velocity profiles deduced from video of the advection of the dye released by the thymol blue technique. In Figure 14a $\delta_I/\delta_M = 1.42$. Also shown on the figure is the linear solution. The qualitative agreement is good, but the theory predicts larger velocities throughout. In Figure 13b $\delta_I/\delta_M = 2.14$, well into the nonlinear range. The flow adjacent to the island is still northward. The interior flow is wavy, but all to the south. The wavy features in Figure 13b have a wavelength $\lambda \approx 4.5\delta_I = 4.5(U_S/\beta)^{1/2}$. This is comparable to the wavelength $\lambda = 2\pi(U/\beta)^{1/2}$ for stationary Rossby waves in a zonal flow U. The discrepancy is because in the experiment the zonal component of the Sverdrup flow is less than U_S.

The meridional transports calculated from zonal integration of the velocity profiles are shown in Figure 14. The transport values are normalized by the linear Island Rule transport, $D\psi_I$, from (2.24). None of the measured profiles extended all the way to the

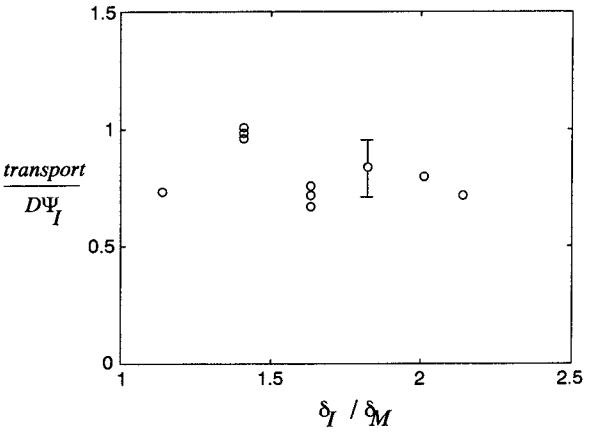

Figure 14. Measured meridional transports to the east of the island normalized by the linear Island Rule transport $D\psi_I$, versus δ_I/δ_M.

eastern boundary so in the transport estimates the last velocity value ($x/r_0 = 0.8$–0.9) was extrapolated to the boundary. No account for the eastern viscous boundary layer is made in either the theory or the measurements. The results are scattered but indicate an average transport of approximately 0.8 times the linear Island Rule independent of $\delta_I/\delta_M < 2.14$. Measurements for values larger than 2.14 were difficult due to the faster and wavy nature of the flow. When the small, but finite, width of the island is accounted for in the calculation of ψ_I from (2.8) and (2.23) the normalized transports in Figure 14 are increased by a factor of 1.12, giving an average transport of about 0.9.

4. Numerical studies: The sliced cylinder

a. The model configuration and forcing

The numerical model used in this study is based on the Miami Isopycnal Coordinate Ocean Model (MICOM) documented by Bleck *et al.* (1992). The model solves the primitive equations of motion using an isopycnal vertical coordinate. The MICOM solves prognostic equations for the isopycnal-layer-averaged quantities of horizontal momentum, layer thickness, and conservation equations for temperature and salinity. A number of simplifying assumptions have been made for the present study. The temperature and salinity are constant within each isopycnal layer so the model effectively carries only the potential density field. There is only one active layer, so that the pressure gradient is due only to variations in the surface elevation. The model has been made adiabatic by turning off the diapycnal mixing and surface buoyancy forcing. The only forcing in the system is a body force parameterization of surface wind stress. Because the model solves for the free-surface height there is no need to independently specify the pressure on the island, as is required for models that make the rigid-lid approximation. Hence our numerical

calculation of ψ_I yields an independent test of the validity of the Island Rule as determined from (2.5).

The horizontal-momentum equation with no cross-isopycnal mass flux simplifies to

$$\frac{\partial \mathbf{v}}{\partial t} + \nabla \frac{\mathbf{v}^2}{2} + (\zeta + f)\mathbf{k} \times \mathbf{v} + \nabla_\alpha M = -g \frac{\tau}{\Delta p} + (\Delta p)^{-1} \nabla \cdot (A \Delta p \nabla \mathbf{v}) - c_D \mathbf{v}, \quad (4.1)$$

where $\mathbf{v} = (u, v)$ is the horizontal-velocity vector, p is the pressure, $\mathbf{k}$ is the vertical-unit vector, $\zeta = \partial v/\partial x - \partial u/\partial y$ is the relative vorticity, $M = gz + p\alpha$ is the Montgomery potential, α is the specific volume of the layer (constant), Δp is the pressure thickness of the layer, and A is an eddy viscosity coefficient. The β-plane approximation is used here, with $f = f_0 + \beta y$. The model is forced with a wind stress of strength τ. Subgridscale processes are parameterized in the model through a Laplacian diffusion of momentum and a linear bottom drag of strength c_D. The lateral boundary conditions are no-slip for momentum and no-flux for density.

In the absence of cross-isopycnal mass fluxes, the continuity equation is represented as a prognostic equation for the layer thickness Δp,

$$\frac{\partial \Delta p}{\partial t} + \nabla \cdot (\mathbf{v} \Delta p) = 0. \quad (4.2)$$

For the present application with no surface buoyancy forcing, no cross-isopycnal mass flux, and uniform temperature and salinity within each layer, the conservation equations for these thermodynamic variables maintain constant values within each layer and thus are not presented here. The complete model equations, and details about the numerical methods used to integrate the equations, can be found in Bleck *et al.* (1992).

The model domain is a circle of radius $R_B = 1000$ km and depth $D = 1000$ m. The potential density of the single active layer is $\sigma_\theta = 25.5$, giving a barotropic deformation radius of $R_d = 1000$ km. Note that in a steady state, the flow should be independent of the magnitude of the deformation radius. The horizontal grid resolution is 20 km unless otherwise noted. The Coriolis parameter at the central latitude of the basin is $f_0 = 10^{-4}\ s^{-1}$, with a meridional gradient $\beta = 1.25 \times 10^{-13}\ cm^{-1}\ s^{-1}$. This value of β gives a meridional variation of $0.25 f_0$ from the southern latitude of the model domain to the northern latitude, equivalent to the effect of the sloping bottom in the laboratory experiments.

We first apply the numerical model to the problem of the sliced cylinder for comparison with the linear solution presented in Section 2 and the lab experiments presented in Section 3. The linear solution provides a useful benchmark for the model calculations in the weak forcing limit. The lab experiment provides a reference for the behavior in the nonlinear system, although exact comparisons are not attempted due to differences in forcing and the lack of fully resolved boundary layers by the finite resolution of the model. Faithful representations of these linear and nonlinear regimes by the model give us confidence in

extending the model solutions into configurations for which it is either not practical or possible to obtain solutions in the lab or in closed form.

The model is forced with a uniform wind stress curl given by

$$\tau_x = \tau_{max} \sin(\theta) \frac{r}{R_B} \qquad \tau_y = -\tau_{max} \cos(\theta) \frac{r}{R_B}, \tag{4.3}$$

where τ_{max} is the maximum wind stress, R_B is the radius of the basin, $r = \sqrt{x^2 + y^2}$, $\theta = \tan^{-1}(y/x)$, and x and y are the zonal and meridional coordinates. For positive τ_{max}, the wind stress is anticyclonic with a downward Ekman pumping velocity.

The strength of the wind forcing is determined indirectly by the specification of the inertial boundary-layer width

$$\delta_I = \left(\frac{\tau_{max}}{\rho_0 R_B D \beta^2} \right)^{1/2}, \tag{4.4}$$

while the strength of the subgridscale mixing is controlled through the thickness of the Munk layer

$$\delta_M = \left(\frac{A}{\beta} \right)^{1/3}. \tag{4.5}$$

The inertial and Munk-layer thickness will be treated as the independent variables that control the model forcing and dissipation. The degree of nonlinearity of the model solutions will be varied by changing the ratio δ_I/δ_M, with all other model parameters being held fixed.

The bottom drag in the model is a parameterization of the bottom Ekman layer in the lab experiment. The strength of the linear bottom drag can be expressed in terms of the Stommel layer δ_s and the Munk layer δ_M as

$$\frac{\delta_s}{\delta_M} = \frac{1}{D} \left[\frac{2 f_0 \delta_M}{\beta} \right]^{1/2}. \tag{4.6}$$

Using the appropriate values for the lab experiment, $\delta_s/\delta_M = 0.678$. The Munk-layer thickness for the numerical experiments has been chosen to match that used for the analytic solutions presented in Section 2, $\delta_M = 39.4$ km, giving $\delta_s = 26.72$ km. The linear bottom drag coefficient C_D is $\delta_s \beta = 3.35 \times 10^{-7}\ s^{-1}$.

b. Meridional island

The transport streamfunction for a thin island oriented in the north-south direction is shown in Figure 15 for several values of δ_I/δ_M. The linear regime in Figure 15a compares well with both the analytic solution in Section 2 and the flow pattern depicted by the tracer distributions in the lab experiment in Section 3. As the nonlinearity is increased, we see a

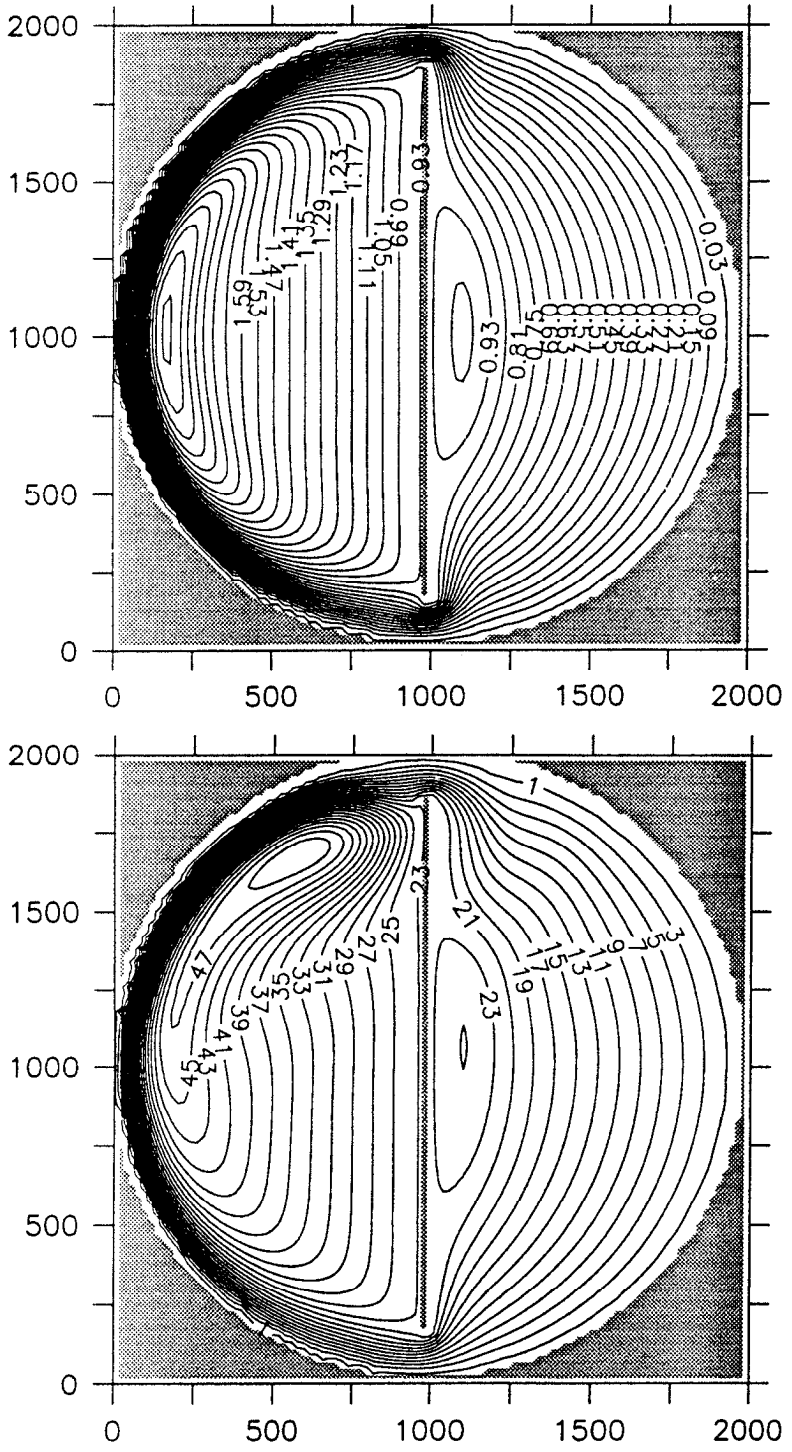

Figure 15. Transport streamfunction (10^6 m^3 s^{-1}) for a thin meridional island with uniform wind stress curl (a) $\delta_I/\delta_M = 0.25$, (b) $\delta_I/\delta_M = 1.25$, (c) $\delta_I/\delta_M = 2.0$.

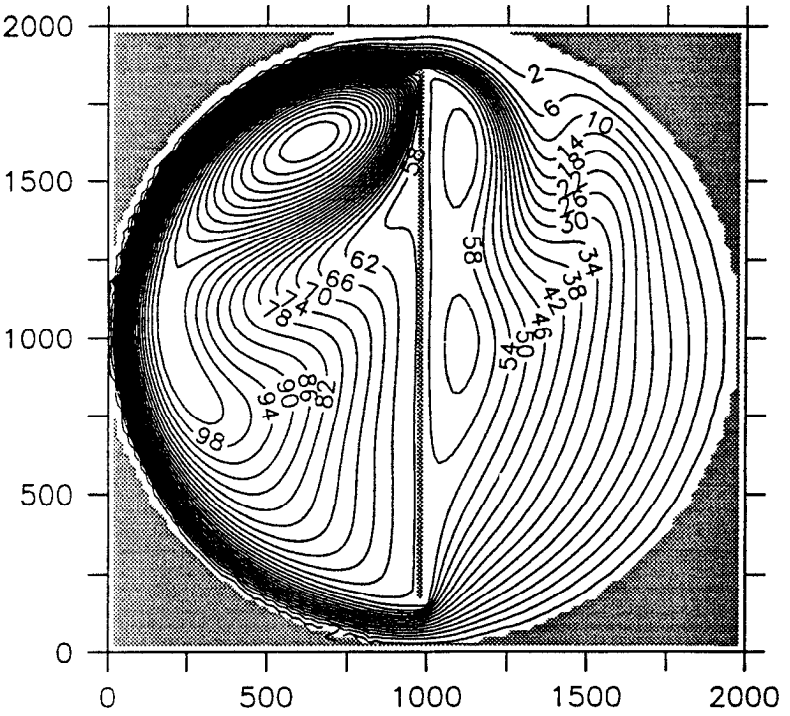

Figure 15. (Continued)

separation of the boundary current near the northern tip of the island (Fig. 15b), similar to that found in the nonlinear lab experiments. The recirculation is slightly asymmetric, with the southern part of the recirculation extending farther toward the tip of the island than the northern part.

For the strongly nonlinear case with $\delta_I/\delta_M = 2.0$, a second recirculation gyre appears near the northern end of the island, within the region of the separated western boundary current. This second local recirculation is connected to the linear recirculation to the south to form a very long recirculation gyre with northward flow along most of the eastern side of the island, consistent with the lab experiments in Figure 11c. The northern recirculation gyre now supplies an anticyclonic frictional stress on the island (a stress that would induce an anticyclonic circulation around the island in the absence of any other forcing), which is the same sense as the stress supplied by the linear recirculation gyre. The balance of terms in the momentum equation indicate that this increased anticyclonic stress is now balanced by a stronger cyclonic stress supplied by the frictional boundary layer along the southeastern portion of the island. There is also a smaller, but not negligible, frictional effect due to the recirculation gyre near the northwestern portion of the island. The highly nonlinear solution is steady, and contains a standing wave pattern east of the island with wavelength similar to that shown in Figure 11c.

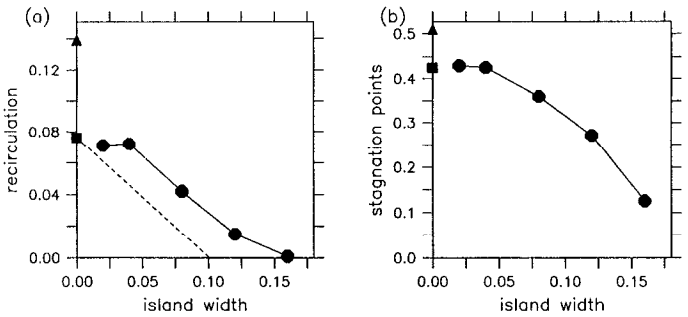

Figure 16. Comparison of (a) the strength of the recirculation gyre (normalized by the maximum streamfunction) and (b) the location of the stagnation points (normalized by the basin radius) for the primitive equation model (circles), the theoretical calculation without (triangle) and with (square) the viscous eastern boundary layer and a finite-thickness Munk layer on the eastern side of the island. The dashed line represents the expected decay of the recirculation strength resulting from the tangential wind stress around the finite-thickness island (Eq. 4.7). All of these calculations are in the steady, linear regime.

A detailed comparison between the analytic solution and the model results in the linear regime reveals some subtle issues that influence the quantitative value of the recirculation strength. The model contains a viscous eastern boundary layer, a finite-thickness Munk layer on the eastern side of the island, and has an island of finite width. While these complicating factors do not invalidate the underlying principle that gives rise to the recirculation in the linear theory, they must be considered in order to obtain a quantitatively accurate estimate of the strength of the recirculation.

This theoretical recirculation strength is compared to that found in the model as a function of the island width (normalized by the basin radius) in Figure 16a. For narrow islands, the model recirculation is very close to that of the analytic solution. The finite Munk layer thickness of the western boundary layer and the inclusion of the weak viscous eastern boundary layer both lead to a decrease in the strength of the recirculation gyre. The strength of the recirculation calculated from the linear theory in the absence of these viscous layers is indicated on the figure by the triangle. A somewhat surprising result found in the model, however, is that as the width of the island increases, the strength of the recirculation gyre decreases such that the recirculation is eliminated for islands wider than $0.15R_B$. The cause of this decrease can be understood if we consider the circulation integral discussed in Section 2. In the development of Eq. (2.8), it was assumed that the tangential wind stress curl across the island was zero. This would be the case if the island were infinitely thin, however, for finite-thickness there is a small but nonzero wind stress tangential to the island. This stress contributes to the integral along the western edge of the island as well as along the northern and southern tips of the island along the contour C. The sense of the circulation induced by the anticyclonic wind stress is to reduce the strength of the linear recirculation gyre. The strength of the circulation induced by the wind stress can

be written, for the wind forcing in Eq. (4.5), as

$$\frac{\psi'}{\psi_I} = 0.75\frac{l}{r_0}, \tag{4.7}$$

where l is the island width, ψ' is the change in the circulation around the island, and ψ_I has been approximated as the Sverdrup transport east of the island at $y = 0$. This decay of the recirculation strength with increasing island width is shown in Figure 16a by the dashed line. The slope agrees well with the decay found in the model, although there is a slight offset that is probably due to corner effects on the island.

The locations of the stagnation points in the model calculations are compared with the analytic solution in Figure 16b. Once again, there is close agreement for narrow islands, but the model calculation departs from the analytic solution as the island width increases. The influences of the finite Munk layer thickness and the finite island width are to shift the stagnation points toward the center of the island, consistent with the weakening strength of the recirculation gyre.

The case of the meridional island in the sliced cylinder with uniform wind stress curl provides a difficult test for the model. Careful consideration of features that are formally of small amplitude is necessary to get a close comparison between the model and the theory. In this particular case, the recirculation gyre is weak because it arises entirely from the small curvature of the eastern boundary (no variation in wind stress curl) and is thus of the same order of magnitude as the modifications to the recirculation strength that result from the viscous effects. We can anticipate that these additional considerations will play a much weaker role for cases in which the recirculation gyres are forced by large-scale variations in the wind stress curl, as is the case for the examples discussed in Section 5.

5. Frictional and inertial effects

In order to further explore the effects of friction and inertia we now depart from the sliced cylinder geometry and discuss a number of numerical experiments with special geometry and forcing. To keep the number of geometrical parameters as simple as possible, we use a rectangular island of zonal extent $L = 2L_x$ and meridional extent $y_n - y_s$ lying in a square, 2000 km $\times$ 2000 km ocean, as shown in Figure 17a. The wind stress curl is confined to patches lying to the east or west of the island, as shown in Figures 17b–d. The most common situation is for the patch to lie to the east of the island as shown in Figure 17b or 17c. In this case:

$$\begin{aligned} &= \tau_0 && (y \geq y_2, x \geq x_t) \\ \tau^{(x)} &= \frac{\tau_0}{2}\left[1 + \cos\left\{\frac{\pi(y_2 - y)}{(y_2 - y_1)}\right\}\right] && (y_1 \leq y \leq y_2, x \geq x_t) \\ &= 0 && (\text{otherwise}), \end{aligned} \tag{5.1}$$

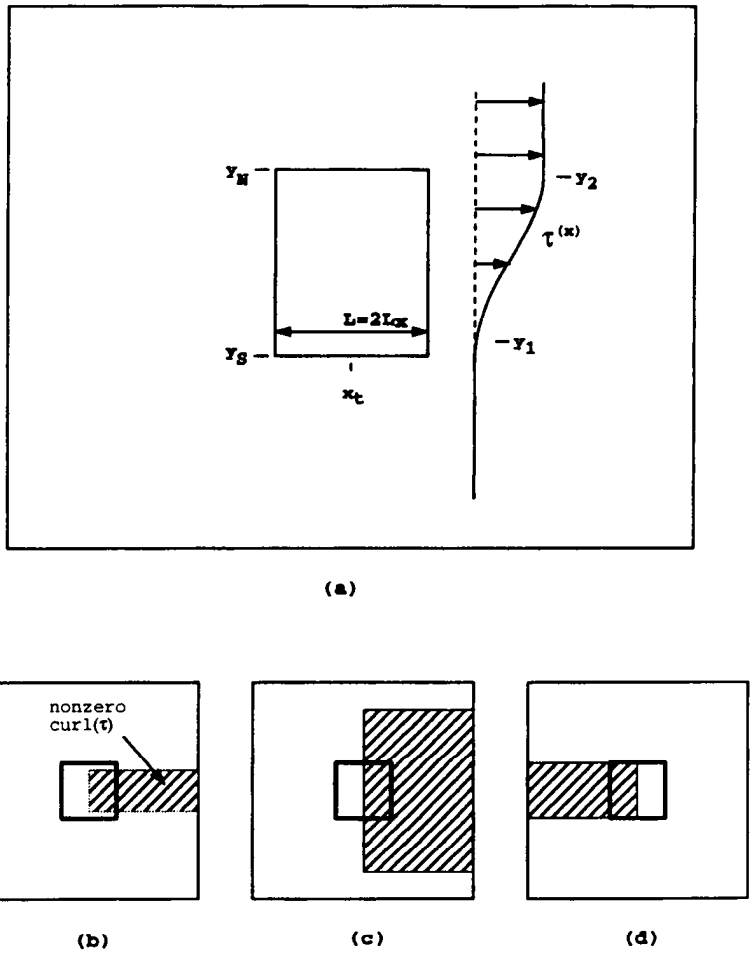

Figure 17. Wind stress distributions for various numerical runs (a, b, c, d).

and $\tau^{(y)} = 0$. When the wind stress curl patch lies to the west of the island, as in Figure 17d, the wind stress is given by (5.1) with the x-dependence changed to $x \leq x_t$.

The parameters governing all numerical runs discussed in this section are listed in Table 1.

a. Inertia

The divergence of vorticity flux over the area enclosed by C, as measured by (2.10), is assumed small in the Island Rule approximation. Nonlinear processes such as boundary current separation or eddy shedding from the island or from unstable island boundary currents are potential sources of vorticity flux. These physical features can generally be

Table 1. Summary of runs quoted in Section 5* (See Figs. 17 and 22 for definitions).

Run	y_1 (km)	y_2 (km)	y_n (km)	y_s (km)	L (km)	Δ (km)	Wind Type Figure 17 b, c, or d	δ_M (km)	δ_I (km)	(Time-Average Direct ψ_I)/ (Island Rule ψ_I)	Comment
1c	700	1300	1390	610	380	600	d	20	30	0.93	Wind Curl West of Island
1cc	700	1300	1390	610	380	600	d	20	45	0.9	Wind Curl West of Island
1d	700	1300	1390	610	380	600	b	20	50	0.89	
1e	700	1800	1390	610	380	600	c	20	30	1.08	
1f	700	1800	1390	610	380	600	c	20	20	1.00	
1g	1200	1800	1890	1110	380	80	b	20	20	0.88	Thin Gap
1h	1240	1840	1930	1150	380	40	b	20	20	0.78	Thin Gap
1i	1260	1860	1950	1170	380	20	b	20	20	0.58	Thin Gap
1k	1260	1860	1950	1170	100	20	b	20	20	0.77	Thin Gap
1l	500	1500	1390	610	380	600	c	20	40	0.84	Thin Gap
1m	1260	1860	1950	1170	380	20	b	40	40	0.19	Thin Gap
1n	700	1300	1390	610	380	600	b	40	68	0.76	
1o	700	1300	1390	610	380	600	b	40	80	0.74	
1p	700	1300	1390	610	380	600	b	40	100	0.72	
1q	700	1300	1390	610	380	600	b	20	20	0.87	
1s	300	1700	1190	810	380	800	+c	90	20	0.84	Zonally Elongated Island
1t	300	1700	1090	910	380	900	+c	90	20	0.86	Zonally Elongated Island
1u	300	1700	1090	910	380	900	c	90	20	0.84	Zonally Elongated Island
1v	300	1700	1050	950	780	940	+c	90	20	0.84	Zonally Elongated Island
1w	300	1700	1050	950	780	940	c	90	20	0.84	Zonally Elongated Island
1x	300	1700	1030	970	780	960	+c	145	20	0.93	Zonally Elongated Island
1y	300	1700	1010	990	780	980	+c	145	20	0.92	Zonally Elongated Island
1z	700	1300	1390	610	380	600	b	40	115	0.70	
4k	700	1300	1390	610	380	600	b	20	35	0.88	Eddy Shedding
4m	300	1700	1010	990	1260	990	+c	40	.25	0.84	Zonally Elongated Island
4n	300	1700	1010	990	1260	990	+c	40	1.0	0.84	Zonally Elongated Island
4o	300	1700	1010	990	1260	990	+c	40	2.5	0.84	Zonally Elongated Island
4p	300	1700	1010	990	1260	990	+c	40	10	0.84	Zonally Elongated Island
4q	300	1700	1010	990	1260	990	+c	40	40	0.66	Zonally Elongated Island
4r	300	1700	1010	990	1260	990	+c	40	25	0.82	Zonally Elongated Island
4s	700	1300	1390	610	380	600	c	20	8	0.89	
4t	700	1300	1390	610	380	600	c	40	30	0.80	
4u	700	1300	1390	610	380	600	c	40	10	0.80	
4v	700	1300	1390	610	380	600	c	20	2	0.88	
5b	700	1300	1390	610	380	600	d	20	20	0.93	Wind Curl West of Island
m1	n/a	n/a	n/a	n/a	1280	990	†	40	10	0.84	Circular Basin
m2	n/a	n/a	n/a	n/a	1280	990	†	40	70	0.57	Circular Basin

*y_1 and y_2 measured from basin southern boundary. See Figure 17 and 22 for other definitions. All runs have $\beta = 2 \times 10^{-13}$ cm^{-1} s^{-1}; $f_0 = 10^{-4}$ s^{-1}, $x_t = 1000$ km, a 2000-km $\times$ 2000-km basin with 20-km grid spacing, and a depth of 1 km.

+The wind stress curl patch is as in Figure 17c but extended over the entire longitude of the basin.

†Uniform curl.

produced by carrying out calculations with sufficiently large δ_I/δ_M. (Unsteadiness occurs at $\delta_I/\delta_M \geq$ about 1.5.)

Figure 18a shows a reference calculation (run 1g, see Table 1) with $\delta_I/\delta_M = 1$ based on $\delta_I = \delta_M = 20$ km and with wind forcing of the type shown in Figure 17b. As shown, the region to the east of the island contains the previously discussed recirculation along with a

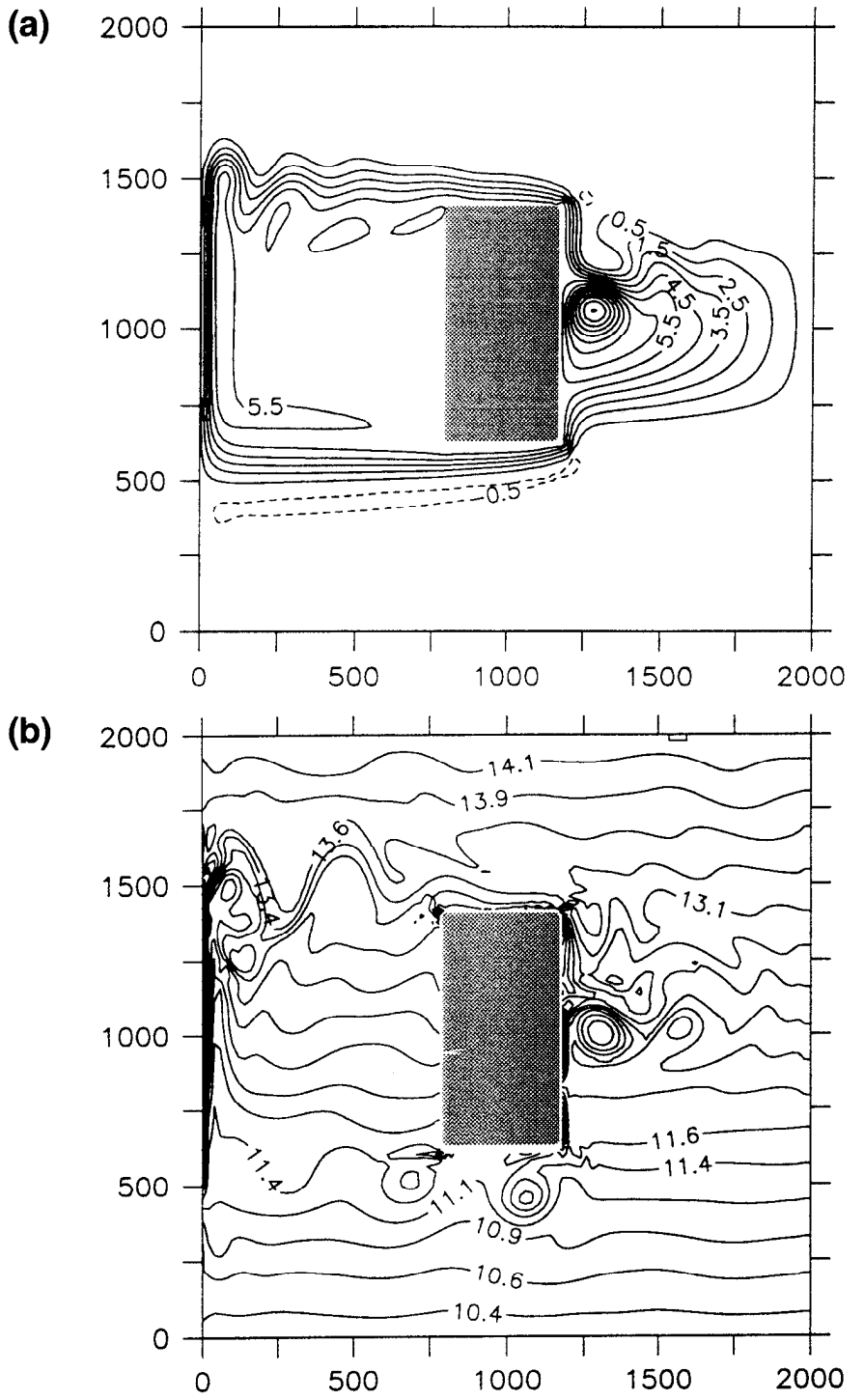

Figure 18. Streamfunction for: (a) Run 1q (δ_I/δ_M = 1.0 and Fig. 17b winds) at t = 900 days; (b) Run 4k, which is the same as (a) but with δ_I/δ_M increased to 1.75 and potential vorticity rather than streamfunction shown at t = 1930 days; (c) Run 1l (δ_I/δ_M = 2.0 with Fig. 17c winds) at t = 1350 days; (d) Run 1d (δ_I/δ_M = 2.5 with Figure 17b winds) at t = 2255 days.

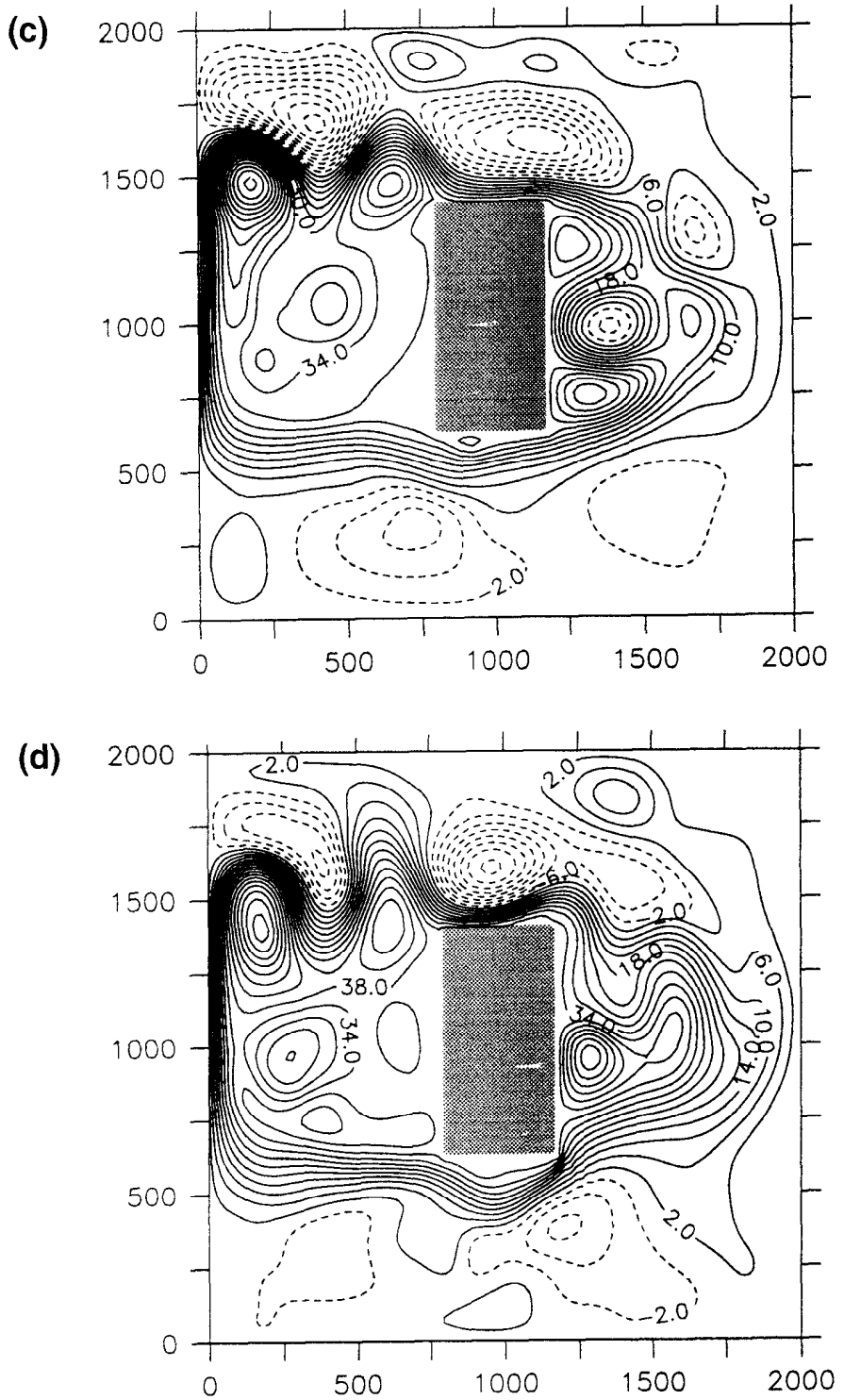

Figure 18. (Continued)

broad, southward Sverdrup flow and a western boundary current. As in some of the sliced cylinder numerical runs, meanders have formed where western boundary currents separate from the island or the ocean boundaries and flow eastward. The observed transport around the island is 88% of the value predicted by the Island Rule (1.2).

If δ_M is held fixed and δ_I is increased beyond about 30 km, which is accomplished here by increasing τ_0, the flow becomes unsteady. (The threshold value of δ_I/δ_M depends upon other parameters such as δ_M/L and this dependence has not been explored.) Figure 18b shows a snapshot of potential vorticity taken from run 4k with $\delta_I = 35$ (or $\delta_I/\delta_M = 1.75$). One of the prominent sources of time dependence is periodic eddy shedding from the southeast corner of the island. The figure shows one eddy forming near the southeast corner, while the previously formed eddy is shown drifting westward near the southwest corner of the island. Other time-dependent features occur in the unstable circulation to the east of the island. Despite these events, the transport around the island is 88% of the value predicted by the Island Rule when an average over a time period long compared to the eddy shedding period is taken. Even instantaneous measurements of the transport are typically within 80–90% of the Island Rule value.

The behavior of the flow close to the eastern island corners is sensitive to the imposed wind stress and, in particular, to the northern and southern extents of the patch. When the patch lies within the latitude band of the island ($y_n > y_2$ and $y_s < y_1$), as shown in Figure 17b, the western boundary current on the east coast of the island tends to stay attached to the eastern boundary. However if the patch extends beyond the latitude band of the island, as shown in Figure 17c, there is a tendency for the flow to separate. This effect is most prominent at the northeastern island corner, where flow approaches from the west in the diffusive boundary current. The current tends to round the corner and stay attached to the coast when winds of the type shown in Figure 17b are imposed, while separation is encouraged when Figure 17c winds are imposed. (Separation is often apparent only in time-dependent flows and is often intermittent, so this interpretation is not always clear.) Figure 18c shows a snapshot from run 11 with $\delta_I/\delta_M = 2$ and $y_2 - y_n = y_s - y_1 = 110$ km. The eastward flow on the northern island boundary clearly separates from the northeast corner, a feature lacking when the original wind stress distribution is used. Although separation is a potential source of vorticity flux, both the time-average and instantaneous transports are 80–90% of the Island Rule value.

Further insight into the separation phenomenon can be gained by considering the northward pressure gradient along the east boundary of the island. On this boundary the y-momentum equation reduces to

$$\frac{\partial}{\partial y}\frac{p}{\rho} = A\frac{\partial^2 v}{\partial x^2}. \tag{5.2}$$

Within the boundary-layer approximation for all δ_I/δ_M, the right-hand side of (5.2) can be shown to be proportional to $\psi_I - \psi^s(x_w(y),y)$, the difference between the Sverdrup and island streamfunctions, by an argument similar to Cessi (1991). Thus, the boundary flow is

driven down a meridional pressure gradient proportional in magnitude to the boundary layer transport. When the wind stress curl patch is extended north and south of the island, as in Figure 17c, the effect is to decrease $\psi_I - \psi^s(x_w(y), y)$ and thus the meridional pressure gradient. Fluid approaching the NE corner of the island along the north boundary feels weaker low pressure to its right as it passes the corner and is less inclined to round the corner and stay attached, as observed numerically.

Further increases in δ_I/δ_M lead to more complex flows, as shown in Figure 18d corresponding to run 1d ($\delta_I/\delta_M = 2.5$ and Fig. 17b winds). Eddies generated by instabilities of complicated origin have increased in size and one, lying to the north of the island, practically fills the gap between the island and the northern ocean boundary. Still the time-averaged transport is 89% of the Island Rule value and instantaneous values are within 80–90%.

One reason for the success of the Island Rule into the range $\delta_I/\delta_M > 1$ is that increased driving of the flow results in increased Sverdrup transport. Although the absolute values of relative vorticity fluxes grow as well, they do not dramatically increase in proportion to the planetary vorticity fluxes (the Sverdrup contribution). In addition, the increasing relative vorticity flux is not accompanied by a divergence of this quantity over the area east of the island. This is in agreement with the general considerations described by (2.10). Both features can be seen by examining the relative contributions of the two terms to the integral around C. Figures 19a–c show the running circulation integrations (c.f., Eq. 2.5) for the cases $\delta_I/\delta_M = 1$ and $\delta_I/\delta_M = 2.5$ discussed above. Only two quantities are shown; the wind stress integral (line with long dashes) and the relative vorticity flux (line with small dashes). The values plotted represent the cumulative integration around the circuit *abcda* shown in the inset. In Figure 19a the relative vorticity flux curve for $\delta_I/\delta_M = 1$ indicates relatively small values everywhere compared to those for the wind stress curve. The main contribution to the relative vorticity flux comes from the northeast extremity of the island, where the boundary current rounds the corner. In Figure 19b, which is based on an instantaneous evaluation of the circulation integral for $\delta_I/\delta_M = 2.5$, the relative vorticity curve shows values which are proportionally larger than the previous case, but still small compared to the ultimate wind stress contribution. The largest contributions come from the two eastern island corners. Almost complete cancellation occurs between contributions from the northern and southern portions of the integration contour, making the total integrated value relatively small. The excursions in the relative vorticity curve for $\delta_I/\delta_M = 2.5$ are diminished by time-averaging, as shown in Figure 19c. Finally, an arrow in each of Figures 19a–c indicates the value of the transport between the island and the basin boundary, as obtained directly from velocities. In each case, the value is close to the final value of the wind stress integration indicating good agreement with the Island Rule.

Given the behavior described above, one might expect the Island Rule to be more vulnerable in situations where the Sverdrup contribution to the total transport is small. Such a case can be arranged by putting the wind stress curl patch to the west of the island, as shown in Figure 17d. It might not be readily apparent that this type of forcing will

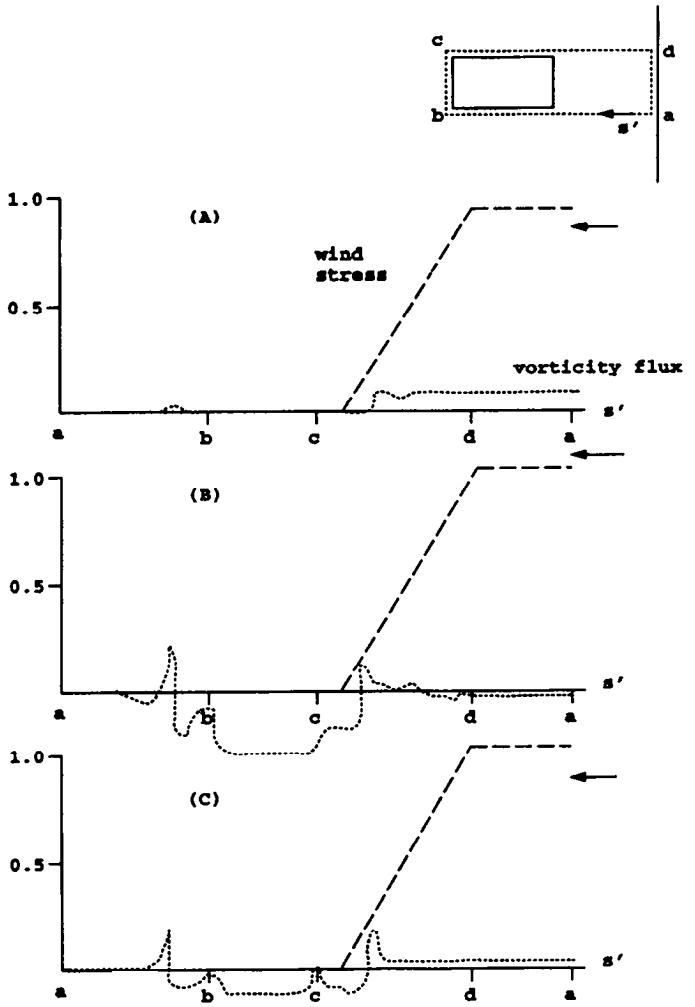

Figure 19. Cumulative integrals of the tangential wind stress ($\int_0^s T \cdot \hat{t}\, ds'$) and normal vorticity flux ($\int_0^s \nu\zeta\, ds'$) around the circuit indicated in the inset. The right-hand end value of the wind stress curve (small dashes) is proportional to the Island Rule transport. The arrow indicates the true transport. (a) Run 1q after steady state is reached, (b) Run 1d at t = 2255, (c) Run 1d values time-averaged over $0 \ll 2255$. All values are normalized by the total value of the circulation integral (i.e., the right-hand side of Eq. 2.5).

produce a circulation around the island, however the presence of a net wind stress on the western halves of the northern and southern island boundaries implies that the dissipation integral around the island is nonzero (c.f., Eq. 2.2). The implication is that fluid must circulate around the island, forming a western boundary layer in which dissipation can occur. Figures 20a,b show two such cases, corresponding to δ_I/δ_M = 1.5 and 2.25 (runs 1c

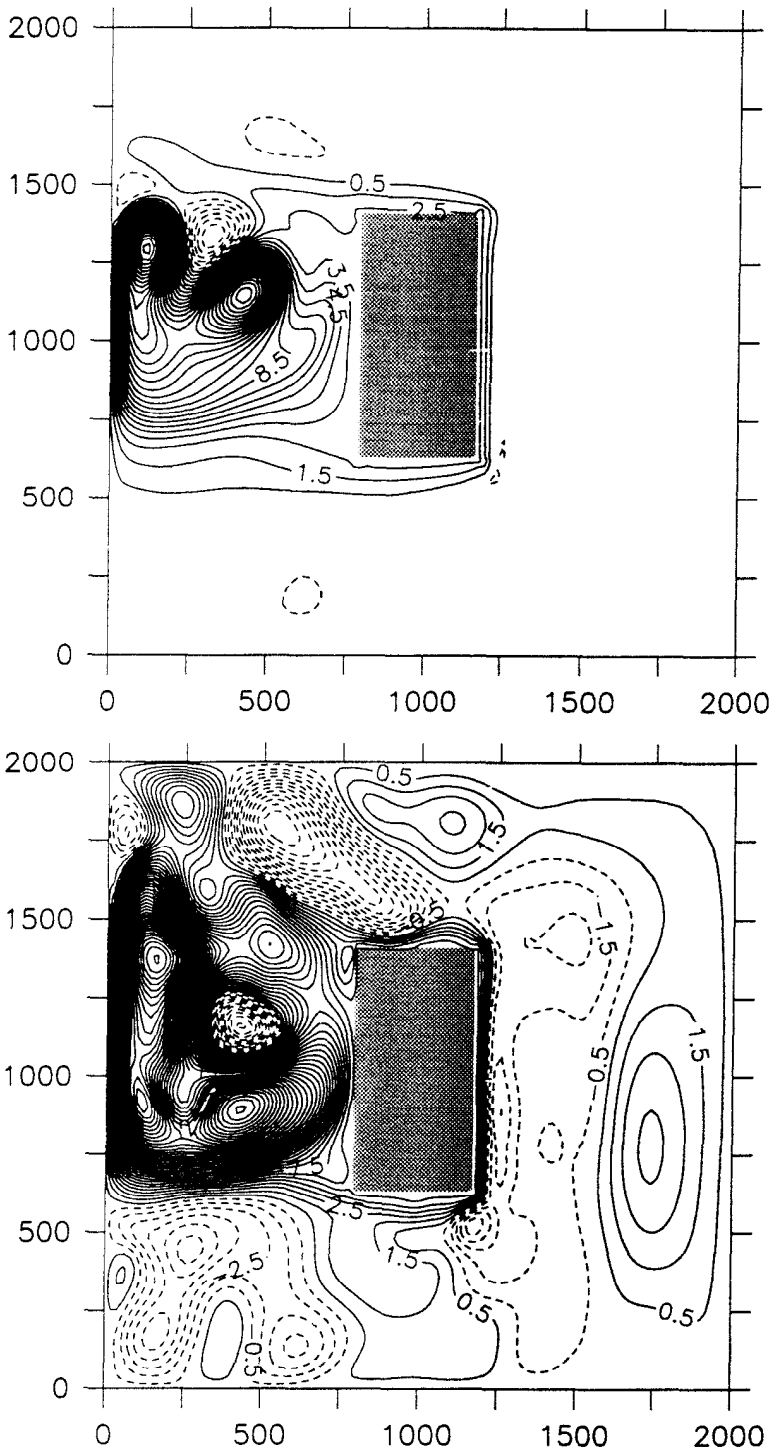

Figure 20. Streamfunction for runs with wind stress curl patch placed to west of island midpoint as in Figure 17d. (a) Run 1c ($\delta_I/\delta_M = 1.5$) at $t = 2220$ days; and (b) run 1cc, which is the same as in (a) but with $\delta_I/\delta_M = 2.5$ at $t = 1395$ days.

and 1cc), respectively. In each case a flow is observed circling the island clockwise. To the north and south of the island the flow is largely contained in the diffusive boundary layers discussed earlier while a western boundary layer carries the southward flow along the east coast of the island. In the case $\delta_I/\delta_M = 1.5$ (Fig. 20a) the flow is steady and the interior region to the east of the island is nearly quiescent. For $\delta_I/\delta_M = 2.25$ the flow is unsteady and this region contains a fluctuating, eddy-driven circulation. As shown in Figure 20b, which is just a snapshot of the flow, the residual circulation to the east of the island is composed mainly of closed streamlines, and thus the increment to the western boundary transport is minimal. The ratio of observed to Island Rule transport is .93 and .95 for the two cases.

The success of the Island Rule in this case can be attributed to the fact the boundary currents hug the wall while rounding the northeast and southeast corners of the island, so that the dominant vorticity flux term over the segments of the contour C, which cut across the western boundary current, is $\nu\partial v/\partial x$. As discussed in connection with (2.10), the x-integral of this term vanishes in the presence of no-slip boundary conditions rendering the total vorticity flux insignificant.

Other runs were made with different values of δ_I/δ_M and δ_M/L and other wind stress contributions. Some of these calculations are described below. Figure 21a contains a summary of the values of (actual transport/Island-Rule-predicted transport) and δ_I/δ_M for each calculation performed. The cases shown are restricted to islands which are well separated from the basin boundary. The calculated transports are generally within about 10–20% of the predicted values over the range $0 < \delta_I/\delta_M < 3.0$. Values $\delta_I/\delta_M > 3.0$. lead to flows which do not appear oceanographically realistic.

In some ways, using the total transport ψ_I as a measure of the Island Rule validity is misleading. As shown in Section 2, the Island Rule ψ_I is composed of a y-averaged Sverdrup streamfunction (c.f., 2.9) and a y-averaged western boundary-layer transport, say $\overline{\psi}_w$. The Sverdrup streamfunction is independent of the island and can be calculated without the aid of the Island Rule. The contribution $\overline{\psi}_w$ is therefore the essential unknown and the Island Rule should be judged on how well it predicts this quantity. Comparisons based on total transport will always be favorable if the contribution from the Sverdrup flow to the east of the island dominates $\overline{\psi}_w$. For example, one could improve the accuracy of the predicted transports simply by moving the eastern basin wall eastward without changing the conditions local to the island.

Figure 21b shows a comparison between the predicted and measured values of $\overline{\psi}_w$ as a function of δ_I/δ_M for a set of numerical experiments using the same island geometry and forcing patterns (runs 1d, 1n–q, 1s, 1t, 4k, 4s–v). Plotted is the difference in predicted and measured $\overline{\psi}_w$ normalized by the y-averaged absolute value of the Island Rule western boundary transport.[2] The small and large dots correspond to runs with $\delta_M = 20$ km and $\delta_M = 40$ km, respectively. The error in $\overline{\psi}_w$ is 10–15% for the $\delta_M = 20$ km, and 20–45% for

2. The y-averaged absolute value of $\psi_w(y)$ is chosen (rather than $\overline{\psi}_w$ itself) as a normalizing factor since $\overline{\psi}_w = 0$ in some island configurations. The meridional ridge is one.

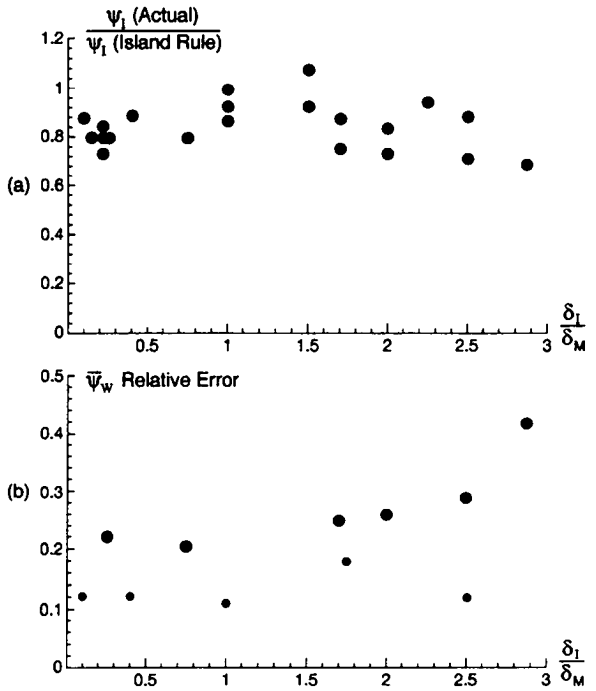

Figure 21. (a) The ratio of actual transport around the island to the value predicted by the Island Rule (1.2) vs. δ_I/δ_M for all numerical runs with islands having $O(1)$ aspect ratios and which are well separated from basin boundaries. (b) Difference between observed and Island Rule, y-averaged western boundary layer transport, normalized by the y-averaged absolute value of the Island Rule western boundary layer transport. Plotted vs. δ_I/δ_M. Small and large dots correspond to δ_M = 20 km and δ_M = 40 km, respectively.

the more viscous δ_M = 40 km cases. The error generally increases as δ_I/δ_M increases, although inspection of the frictional and inertial terms in the circulation integral shows that the errors are almost completely due to frictional effects on the island's north and south boundary and the eastern boundary of the basin. Even in the most extreme case (δ_M = 40 km, δ_I/δ_M = 2.75, run 1d), which has an error of 42%, the relative vorticity flux is negligible compared to net friction. This result suggests that the main influence of nonlinearity on the circulation budget is enhancement of friction rather than production of relative vorticity flux. The frictional enhancement is most pronounced near the eastern corners of the island.

b. Narrow gaps

If the island lies sufficiently close to a continental boundary, side-wall friction within the gap may block the throughflow and reduce the value of ψ_I well below the value predicted by the Island Rule. How small must the gap width Δ be in order for blocking to occur? If the gap separates the island from the ocean western boundary, blocking requires (at the very least) that $\Delta \leq$ the relevant frictional western boundary layer thickness, in this case

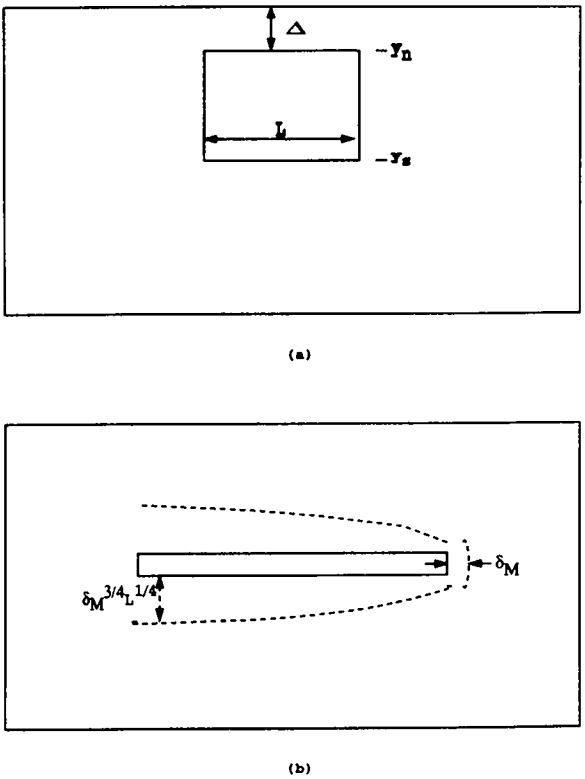

Figure 22. Definition sketches for calculations with thin gaps (a) and zonal elongation (b).

δ_M. Frictional effects along the island western boundary are then potentially as large as those along the island eastern boundary, in violation of the assumption that all dissipation occurs on the island eastern boundary. Wajsowicz (1993a) estimates the reduction in transport, including the case where the western boundary is tilted with respect to the y-axis. In principle, the same considerations apply at an eastern basin boundary.

A more subtle problem arises when the gap separates the island from a north or south boundary (Fig. 22a) as there are two relevant frictional length scales: the diffusive layer width $\delta_M^{3/4}L^{1/4}$ (Fig. 22b) and δ_M. The magnitude of blocking in the gap can be approximated by estimating the contribution of the north island boundary to the dissipation integral in (2.5). For Munk friction the latter is order $LA_H\psi_I/\Delta^3$ while the left-hand term is order $\beta(y_n - y_s)\psi_I$. The ratio of the latter to former is R_Δ^3, where

$$R_\Delta = \frac{\Delta}{\delta_M \alpha^{1/3}}, \tag{5.3}$$

and where α denotes the island aspect ratio $L/(y_n - y_s)$. One therefore expects frictional blocking of the flow to occur for values $O(R_\Delta) \leq 1$.

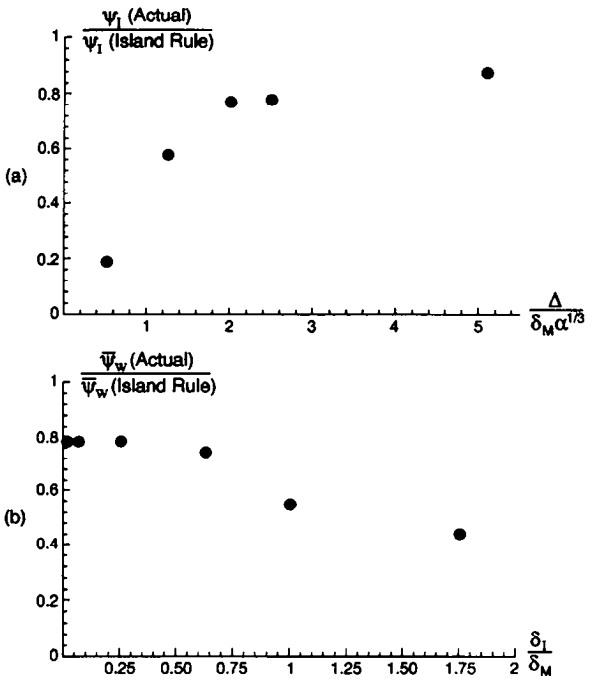

Figure 23. (a) Ratio of actual ψ_I to Island Rule ψ_I vs. gap width parameter for runs 1g–i and 1k–m. (b) Actual western boundary layer transport divided by Island Rule western boundary layer transport for runs 4m–r.

Figure 23a shows the results of a series of calculations in which the value of R_Δ was varied and the ratio of actual transport to Island Rule transport measured. The comparison is based on total transport rather than western boundary-layer transport since the total transport is blocked. It is clear that significant reduction in actual transport occurs only for values of $R_\Delta \leq 1.5$.

c. Zonally elongated island

Section 2iii discussed the violation of the Island Rule which occurs when frictional dissipation along the north or south boundaries grows as large as that in the island's western boundary layer. For a Munk model, this violation can be expected when the thickness $y_n - y_s$ becomes as small as the diffusive boundary layer thickness $\delta_M^{3/4} L^{1/4}$ (see Fig. 22b), or

$$R_z = \frac{y_n - y_s}{\delta_M^{3/4} L^{1/4}} \leq 1. \tag{5.4}$$

In such cases the value of ψ_I for linear circulation is expected to obey our modified Island Rule (2.40), provided that the wind stress curl is a function only of latitude. In particular,

(2.40) predicts an island western boundary layer transport which is 80% of the value predicted by the original Island Rule.

In an attempt to verify this prediction, we have carried out a sequence of calculations (runs 4m–r) based on $\delta_M = 40$ km, $l = 1260$ km, $y_n - y_s = 20$ km, corresponding to $R_z = .21$. The wind stress corresponds to that of Figure 17c but extended across the entire longitude of the basin. Figure 23b shows the western boundary layer transport $\overline{\psi}_w$ normalized by the Island Rule value as a function of δ_I/δ_M. For $\delta_I/\delta_M < .3$, the expected ratio 0.80 is obtained to within 1% error. The ratio decreases as δ_I/δ_M grows and inspection of the circulation integrals reveals that this is associated with nonlinear enhancement of frictional effects rather than creation of net vorticity fluxes.

Figures 24a,b show numerical solutions for the cases $\delta_I/\delta_M = .25$ and 1.65 (runs m1 and m2, both for zonally elongated islands in circular domains with uniform wind stress curl). In Figure 24a the solution generally resembles the linear solution with the north/south symmetry and stagnation points near the mid-point of the island. The theory leading to (2.40) predicts zero boundary layer transport at $x - x_t = -0.6\, L_x$ and this is in substantial agreement with the model. In Figure 24b, the stronger nonlinearity has led to separation of the eastward flow past the east island tip, destroying the north-south symmetry. The point of zero boundary layer transport on the southern side of the island has shifted all the way to the eastern island tip while that on the northern boundary has shifted to the western portion of the island.

6. Conclusion

Our study of flow around islands has concentrated on identification of characteristic circulation features and their dynamics and on the validity of the Island Rule. One of the most striking features noted is a recirculation gyre lying to the immediate east of the island. The recirculation can form when the Sverdrup streamfunction at the island's eastern boundary reaches a minimum or maximum within the latitude band of the island. Thin meridional ridges particularly favor recirculation formation, a consequence of the requirement of zero net dissipation around such an island. The positions of the stagnation points marking the gyre extremities can be predicted by a linear calculation based on Stommel or Munk dynamics. The gyre recirculation is closed only to leading order; net Ekman suction or pumping leads to an $O(\beta(y_n - y_s)/f)$ volume flux across the otherwise closed recirculation gyre boundary and shifts in the positions of the stagnation points, both of which can be calculated. The results of linear theory generally agree with sliced cylinder laboratory experiments and primitive equation numerical simulations provided δ_I/δ_M is less than about 1.5 (agreement is found even for $\delta_I/\delta_M = O(1)$).

Evidence of recirculation patterns near the eastern faces of island and abyssal ridges has been discussed by several authors. Ridgway and Godfrey (1994, their Figs. 2a,b) suggest a circulation in the upper 2000 m to the east of Australia with closed streamlines resembling the recirculation described in this paper. The region in question is topographically complex and lies partially in the westward shadow of other islands such as New Zealand, making

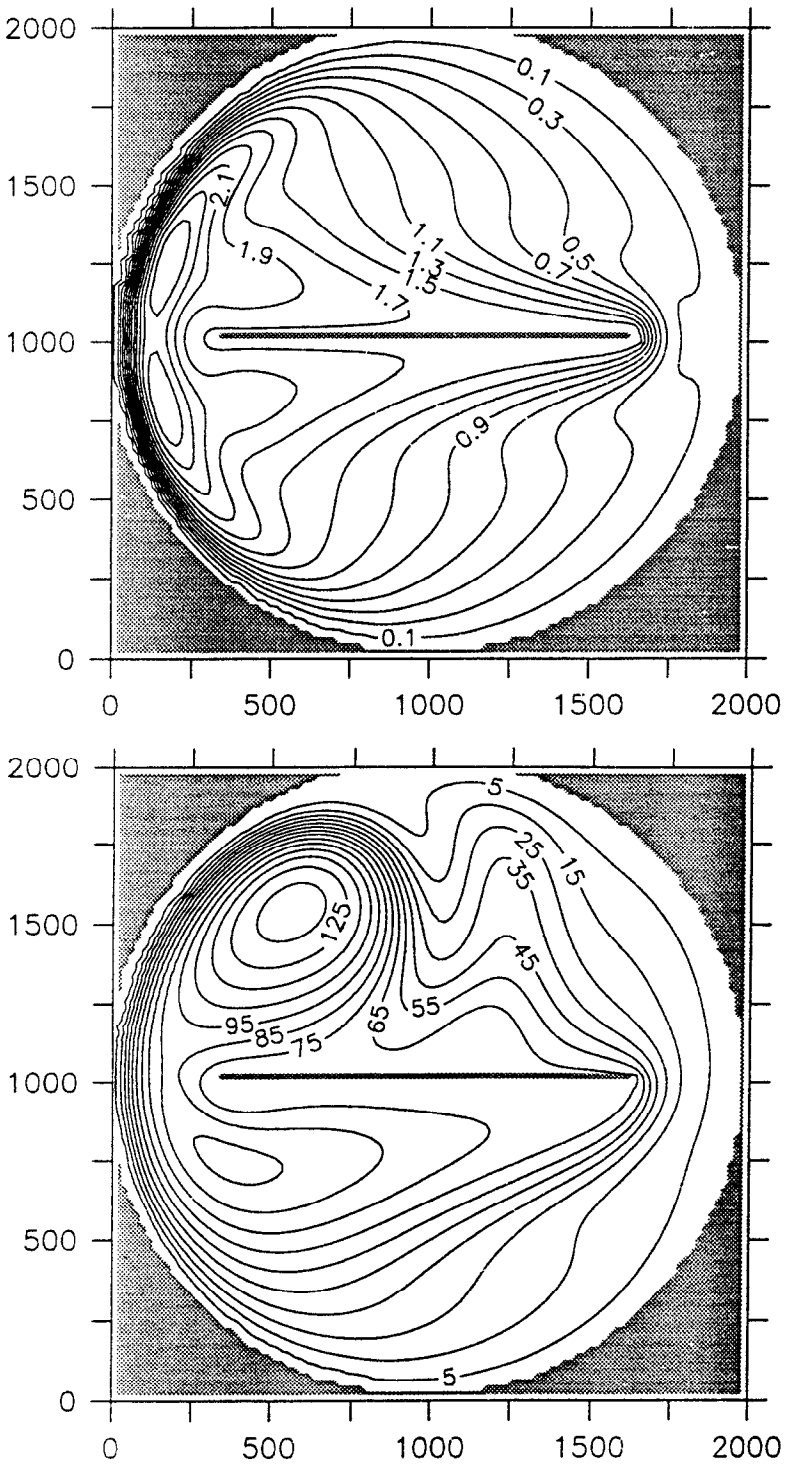

Figure 24. Streamfunction for runs m1 ($\delta_l/\delta_M = 0.25$) and m2 ($\delta_l/\delta_M = 1.75$).

closer comparison with our simple model problematic. An abyssal recirculation to the east of the Mid-Atlantic Ridge is suggested in Friedrichs and Hall (1993, their Fig. 10).

Other linear circulation features include diffusive boundary layers which form on the island's north and south boundaries and which are continuations of the western boundary layer on the island's eastern coast. The diffusive layers widen westward at a rate proportional to the quarter-power of the distance from the island's eastern corners under Munk dynamics (and to the half-power under Stommel dynamics). These boundary layers detach once the western corners of the island are reached and extend to the basin's western boundary as zonal jets. Our laboratory and numerical experiments have verified that the island's western boundary current does continue around corners and into the diffusive layers, and then eventually into zonal jets west of the island for δ_I/δ_M less than about 1.5. This occurs even in the case of a meridional ridge.

For $\delta_I/\delta_M > 1.5$ the diffusive boundary layer flow feeding the island's boundary layer on its eastern side may detach and protrude into the Sverdrup region to the east of the island. The threshold value of δ_I/δ_M for separation varies somewhat between the laboratory and numerical experiments and is sensitive to the wind stress distribution. We have not resolved these differences; however, we have found that separation is encouraged when the local north-south pressure gradient on the (ageostrophic) western boundary is weakened by the local value of the wind stress curl.

Separation of the western boundary current itself is also observed in the same parameter range and the detached flow can be pooled into eddies which are intermittently shed from the island. Other sources of time dependence arise including instabilities of the various western boundary layers and their extensions. Despite the presence of such features, the net vorticity fluxes around the integration contour, C, do not grow large enough to cause major violations of the linear Island Rule, at least not for $\delta_I/\delta_M < 3.0$ and no-slip boundary conditions. We attribute this resilience to the fact that the island's western boundary layer produces no net vorticity flux to leading order and to the lack of needed correlations between u and v in the waves and eddies generated to the east of the island. One caveat should be mentioned: if free-slip boundary conditions are used, it is no longer true that the boundary-layer vorticity flux vanishes, and this could lead to more significant violations of the Island Rule.

We have described two situations in which dissipation becomes important along the northern or southern boundaries and alters the Island Rule accordingly. The first arises when the island is placed within a distance of $O(\delta_M \alpha^{1/3})$ of the northern or southern basin boundary, in which case blockage of the circulation around the island occurs. Using the numerical model, we have demonstrated the reduction of ψ_I when the gap thickness Δ is reduced beyond about $1.5\delta_M\alpha^{1/3}$. The dependence upon the ⅓ power of the island aspect ratio $\alpha = L/(y_n - y_s)$ indicates insensitivity to the island shape. The Stommel model counterpart to this calculation was not explored numerically but the critical gap thickness is projected to be $\alpha\delta_s$.

The second situation occurs when the island is zonally elongated to the point where dissipation along the north or south island boundaries grows as large as the dissipation in the boundary layer on the island's east side, violating a key Island Rule assumption. This occurs when the north/south boundary layer thickness, $(\delta_s L)^{1/2}$ or $\delta_M^{3/4} L^{1/4}$, exceeds the island longitudinal thickness $y_n - y_s$. In such cases, the extra dissipation can be accounted for analytically and the original Island Rule altered accordingly, as we have done for the case of x-independent wind stress curl. Whereas the Godfrey theory (1.2) predicts that all Sverdrup flow approaching the island from the north or south is diverted around the island to the east, our new result predicts that 20% of this flow is diverted to the west under Munk dynamics (and 33.3% under Stommel dynamics). The implication is that stagnation points arise on the north and south island boundaries. The new transport prediction has been verified to within 1% in a series of numerical experiments with a zonally elongated island with $L = 1260$ km, $y_n - y_s = 20$ km and $\delta_I/\delta_M < .25$. Larger values of δ_I/δ_M cause further increases in the proportion of flow diverted to the west of the island.

In summary, total transports agree within 75% of values predicted by the Island Rule as long as the island is well separated from all basin boundaries. Even in the previously discussed case of zonally elongated islands with linear dynamics (for which a key Island Rule assumption fails), the transport prediction is still close to the true value. We also find that violations are primarily due to the presence of dissipation over contour C. Nonlinearity does not generally produce net vorticity fluxes large enough to significantly change the transport, but there is an interesting enhancement of friction with increasing δ_I/δ_M which is significant. Relative errors in transport prediction are more significant when measured using island western boundary layer transport. These errors rarely exceed 40% in our calculations but could be much higher if larger values of δ_M were used.

There are too many interesting extensions and complications of our idealized barotropic model to list. However, one which is particularly obvious is stratification. As shown in the Appendix, the contribution of nonlinear advection to a two-layer circulation integral can be written as a net potential vorticity flux, a quantity associated with baroclinic instability. It is possible that baroclinically unstable currents in a stratified ocean might succeed where our barotropic currents failed in producing fluxes of significant magnitude to change the circulation balance.

Acknowledgments. This work was supported by the National Science Foundation under grant nos. OCE-93-01323, OCE-93-01845, OCE-95-02083, OCE-95-20302 and OCE-96-16949. The authors would like to thank Stuart Godfrey, Roger Samelson and an anonymous reviewer for their helpful suggestions. This is Woods Hole Oceanographic Institution contribution no. 9429.

APPENDIX

The Island Rule for a stratified fluid

It is straightforward to generalize the arguments in Section 2 to a stratified fluid. We start be considering a layer model of the classical type which is governed by quasi-geostrophic

dynamics. If each undisturbed layer thickness is H_j then for each layer j, the integral of the momentum equation around the contour C, defined as before, yields,

$$\oint_C H_j \frac{\partial \boldsymbol{u}_j^{(0)}}{\partial t} \cdot \hat{\imath}\, ds + \oint_C H_j \zeta_j^{(0)} \boldsymbol{u}_j^{(0)} \cdot \hat{n}\, ds + \oint_C \beta y \boldsymbol{u}_j^{(0)} H_j \cdot \hat{n}\, ds + \oint_C H_j f_0 \boldsymbol{u}_j^{(1)} \cdot \hat{n}\, ds = \oint_C [\boldsymbol{T}_j + \mathscr{F}_j] \cdot \hat{\imath}\, ds. \tag{A.1}$$

where variables with a superscript $^{(0)}$ are the geostrophic velocities and those with superscript $^{(1)}$ are of one higher order in Rossby number. $\mathscr{F}_j$ and $\boldsymbol{T}_j$ are the dissipation and forcing terms, respectively, for layer j. The expansion of the momentum equation in a series of Rossby number is a standard development and can be found, for example in Pedlosky (1987). The lowest order balance yields the geostrophic approximation and the next order yields the momentum equation whose integral is used in (A.1). The integral of the mass conservation equation around the same contour, yields,

$$H_j \oint_C \boldsymbol{u}_j^{(1)} \cdot \hat{n}\, ds = -\int\int_R \frac{\partial h_j^{(0)}}{\partial t}\, dx\, dy - \oint_C \boldsymbol{u}_j^{(0)} h_j^{(0)} \cdot \hat{n}\, ds, \tag{A.2}$$

where $h_j^{(0)}$ is the lowest order departure of the layer thickness from the constant value H_j. Combining (A.1) and (A.2) and using the manipulations introduced earlier for the barotropic problem it is easy to show that the constant $\psi_I(j)$, which varies from layer to layer, i.e., is a function of layer index j, is given for steady flow by:

$$\beta(y_n - y_s)\psi_I(j) = \oint_C \boldsymbol{u}_j^{(0)} q_j^{(0)} \cdot \hat{n}\, ds - \frac{1}{H_j} \oint_C [\boldsymbol{T}_j + \mathscr{F}_j] \cdot \hat{n}\, ds, \tag{A.3}$$

where $q_j^{(0)}$ is the quasi-geostrophic potential vorticity associated with motion

$$q_j^{(0)} = \zeta_j^{(0)} - \frac{f_0 h_j^{(0)}}{H_j}. \tag{A.4}$$

For a stratified fluid it is the flux of potential vorticity which takes the place of the relative vorticity flux in contributing to the determination of the transport around the island, here layer by layer. We showed above that the no-slip condition reduces the importance of the relative vorticity flux but the portion of the flux associated with the flux of layer thickness (heat flux) will be unaffected by that boundary condition. This raises the interesting possibility that baroclinic eddies could give rise to net circulations around the island in layers deeper than those forced directly. This will be a subject for future study.

The generalization of this result to the case of nonquasi-geostrophic flow is rather complex due to the large variations of layer thickness. The most straightforward generalizations lead to complicated and not very useful analogues of (A.3). In one case though, the generalization can be neatly made.

We write the momentum equation for the j^{th} layer in the form

$$\frac{\partial \boldsymbol{u}_j}{\partial t} + \hat{k} \times q_j(h_j \boldsymbol{u}_j) = -\nabla B_j + \frac{1}{h_j}(\mathscr{F}_j + \boldsymbol{T}_j), \tag{A.5}$$

where

$$q_j = \frac{f + \zeta_j}{h_j}$$
$$B_j = \frac{p_j}{\rho_j} + \frac{1}{2}[\boldsymbol{u}_j]^2, \tag{A.6a,b}$$

and h_j is the layer thickness of the j^{th} layer. The potential vorticity is q_j.

We integrate the momentum equation around the contour C where now C wraps around the western side of the island as before but reaches the eastern boundary of the basin via two isolines of potential vorticity, q_n and q_s, which originate from the northern and southern tips of the island but do not necessarily coincide with latitude circles. This assumes that the potential vorticity isolines originating from those two extremities reach the eastern boundary and do not close within the basin. If they do, the following argument fails. If the contours do strike the eastern wall we obtain

$$\int_{q_j=q_n} \hat{n} \cdot \boldsymbol{u}_j h_j q_n \, ds - \int_{q_j=q_s} \hat{n} \cdot \boldsymbol{u}_j h_j q_s \, ds = \oint_C \frac{\partial \boldsymbol{u}_j}{\partial t} \, ds + \oint_C [\mathscr{F}_j + \boldsymbol{T}_j]/h_j \, ds, \tag{A.7}$$

where $\hat{n}$ is the outward unit normal to the northern isoline, q_n, and the inward directed normal to the southern potential vorticity isoline, q_s as shown in Figure 25. We may take q out of the integrals on the left-hand side of (A.7) since q is constant on its isolines. We define the total mass flux across each isoline as M_n and M_s, respectively. Since the mass transport is divergent unless the flow steady, these will in general differ, thus,

$$(q_n M_n - q_s M_s) = -\oint_C \frac{\partial \boldsymbol{u}_j}{\partial t} \cdot \hat{t} \, ds - \oint_C \overline{\boldsymbol{m}_j' q_j'} \cdot \hat{n} \, ds + \oint_C [\mathscr{F}_j + \boldsymbol{T}_j]/h_j \cdot t \, ds. \tag{A.8}$$

We have added a term on the right-hand side of (A.8) to represent the eddy flux of potential vorticity across the contours q_n and q_s should the motion be unsteady and the isolines are isolines of time-averaged potential vorticity. We write M_n and M_s in terms of an average transport around the island, M, and a portion which differs from one isoline to the other, ΔM, which represents a temporary storage of mass in the region and obtain,

$$(q_n - q_s)M = -\oint_C \frac{\partial \boldsymbol{u}_j}{\partial t} \cdot \hat{t} \, ds - \oint_C \overline{\boldsymbol{m}_j' q_j'} \cdot \hat{n} \, ds - \frac{q_n + q_s}{2} \Delta M + \oint_C [\mathscr{F}_j + \boldsymbol{T}_j]/h_j \cdot t \, ds. \tag{A.9}$$

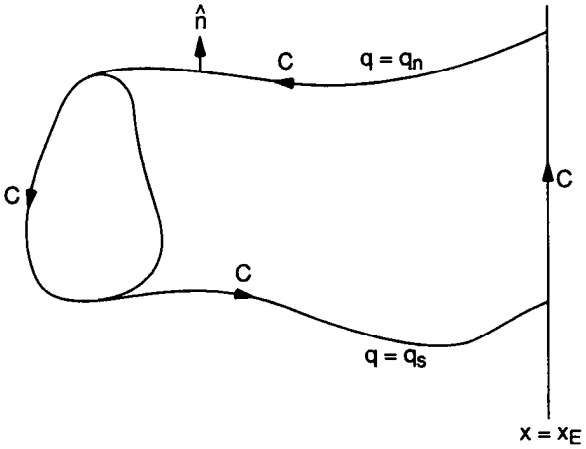

Figure 25. The contour C in the case when it coincides with two isolines of potential vorticity in the j^{th} layer. It is assumed these isolines, which originate from the northern and southern tips of the island reach the eastern boundary of the basin. Note that on the more southern isoline, the unit normal vector is directed inward.

In the time-mean, both the first and third terms on the right-hand side of (A.9) will be zero. Thus the time averaged flux of mass around the island in each layer is given by the direct forcing (which may be small in layers not exposed to surface forcing) and to dissipation (which we expect to be normally weak on C) and to the flux of potential vorticity in the layer across the mean potential vorticity isolines connecting the northern and southern extremities of the island to the basin boundary.

REFERENCES

Bleck, R., C. Rooth, D. Hu and L. T. Smith. 1992. Salinity-driven thermocline transients in a wind- and thermohaline-forced isopycnal coordinate mode of the North Atlantic. J. Phys. Oceanogr., *22,* 1486–1505.

Csanady, G. T. 1978. The arrested topographic wave. J. Phys. Oceanogr., *8,* 47–62.

Cessi, P. 1991. Laminar separation of colliding western boundary currents. J. Mar. Res., *49,* 697–717.

Friedrichs, M. A. and M. M. Hall. 1993. Deep circulation in the tropical North Atlantic. J. Mar. Res., *51,* 697–736.

Godfrey, J. S. 1989. A Sverdrup model of the depth-integrated flow from the world ocean allowing for island circulations. Geophys. Astrophys. Fluid Dyn., *45,* 89–112.

Pedlosky, J. 1968. An overlooked aspect of the wind-driven ocean circulation. J. Fluid Mech., *32,* 809–821.

—— 1974. Longshore currents, upwelling and bottom topography. J. Phys. Oceanogr., *4,* 214–216.

—— 1987. Geophysical Fluid Dynamics. Springer-Verlag, New York, 710 pp.

—— 1994. Ridges and recirculations: Gaps and jets. J. Phys. Oceanogr., *24,* 2703–2707.

Pedlosky, J. and H. P. Greenspan. 1967. A simple laboratory model for the oceanic circulation. J. Fluid Mech., *27,* 291–304.

Qiu, B. D. Koh, C. Lumkin and P. Flament. 1997. On the existence and formation mechanism of the North Hawaiian Ridge Current. J. Phys. Oceanogr., *27,* 431–444.

Ridgway, K. R. and J. S. Godfrey. 1994. Mass and heat budgets in the East Australian Current: A direct approach. J. Geophys. Res., *99*(C2), 3231–3248.

Stewart, R. W. 1964. The influence of friction on inertial models of oceanic circulation, *in* Studies on Oceanography, Papers dedicated to Professor Hidaka in commemoration of his 60th birthday, K. Yoshika, ed., Tokyo University, Geophys. Inst., 3–9.

Wajsowicz, R. C. 1993a. The circulation of the depth-integrated flow around an island with applications to the Indonesian throughflow. J. Phys. Oceanogr. *23,* 1470–1484.

—— 1993b. A simple model of the Indonesian throughflow and its composition. J. Phys. Oceanogr., *23,* 2684–2703.

—— 1996. Flow of a western boundary current through multiple straits: An electrical circuit analogy for the Indonesian throughflow and archipelago. J. Geophys. Res., *101,* 12,295–12,300.

Warren, B. A. and W. B. Owens. 1988. Deep currents in the central subarctic Pacific Ocean. J. Phys. Oceanogr., *18,* 529–551.

Wijffels, S. E., N. Bray, S. Hautala, G. Meyers and W. M. L. Morawitz. 1996. The WOCE Indonesian throughflow repeat hydrography sections: I10 and IR6. International WOCE Newsletter, *24,* 25–28.

Received: *2 January, 1997;* revised: *10 April, 1997.*